R. & M. No. 3486

R. & M. No. 3486

MINISTRY OF TECHNOLOGY

AERONAUTICAL RESEARCH COUNCIL
REPORTS AND MEMORANDA

Low-speed Wind-tunnel Tests on a 1/8th Scale Model of the Handley-Page HP.115

by P. B. E. ENGLER and G. F. MOSS

LONDON: HER MAJESTY'S STATIONERY OFFICE
1967

PRICE 15*s.* 6*d.* NET

Low-speed Wind-tunnel Tests on a 1/8th Scale Model of the Handley-Page HP.115

by P. B. E. ENGLER and G. F. MOSS

Reports and Memoranda No. 3486*
August, 1965

A series of tunnel tests was made on a slender wing design to provide a basis for the flight-tunnel comparison of data and to give general wind-tunnel support for the flight research work on the aeroplane. The interim comparisons with flight which have been possible so far show good agreement as regards lift and lateral and directional stability, but significant differences in some control derivatives.

LIST OF CONTENTS

* Replaces R.A.E. Tech. Report 65 180—A.R.C.27492.

---

1. *Introduction.*

The Handley-Page HP.115 research aircraft was built to enable flight investigations to be made of the low-speed aerodynamic characteristics and handling qualities of slender wing configurations designed for good high speed performance. At supersonic cruise conditions, aircraft with slender wings will usually have attached flow, but at low speeds, for example during take-off and landing, the flow separates from the highly swept leading-edges and the aero-dynamics of the aeroplane tend to be dominated by the strong vortex field above the wing. Since stalling in the conventional sense does not occur and the use of high-lift devices is not at present proposed for this type of wing, the incidence of these wings at low speed conditions is therefore rather larger than with more conventional wing configurations. The comparatively new aero-dynamic features, associated with unconventional inertia characteristics, pointed the need for flight research work, particularly as regards dynamic behaviour and handling.

Associated with the uncertainties of aerodynamic behaviour was the need for a check on the validity of predictions of full-scale aircraft behaviour from wind-tunnel tests. To meet this, a series of wind-tunnel tests were made on a $\frac{1}{8}$th scale model in the R.A.E. 13 ft × 9 ft low-speed tunnel in parallel with the flight-test programme on the aircraft, and the results are reported here. An interim report of the flight tests has been published (Ref. 1) and some interim flight-tunnel comparisons have been possible, particularly as regards overall lateral and directional stability, and control derivatives.

The main series of tunnel tests was carried out between May 1961 and November 1962 in several short stages.

2. *Description of the Model.*

The HP.115 is a slender wing of 75 deg leading-edge sweep with streamwise tips. The wing has a symmetrical biconvex section formed by circular arcs with sharp leading and trailing edges and a thickness-chord ratio of 6 per cent. The cockpit is underslung to limit interference over the forward part of the wing and a fixed undercarriage is fitted. Details of the model are given in Fig. 1 and Table 1. A reasonable representation of the aircraft was made without undue attention to small detail, since the comparison between flight and tunnel data was intended to be fairly representative of normal practice. Care was taken to reproduce the geometry of the elevon hinge accurately (since control hinge-moments were to be measured) and all the major accessories, such as parachute fairings, the pitot-static boom and fixed undercarriage were included. However, the complex control tab configurations used in flight could not be simulated and the undersurface cavities of the (retracted) dive brakes were not represented on the model except for a few check tests. The engine nacelle was made hollow to permit a reasonable amount of intake flow (roughly equivalent to the engine idling case in flight), and check tests with this flow both increased and reduced confirmed that this was not a significant factor on the test results.

The model was constructed of laminated glass-cloth and epoxy-resin and was extremely rigid. No artificial means of fixing transition were employed.

3. *Experimental Details.*

The model was suspended by wires from the overhead mechanical balance in an inverted position approximately 1 ft above the centreline of the tunnel section. The two main cleats, universally jointed, were spaced widely fore-and-aft along the longitudinal axis of the model and the rearmost of these acted as the incidence pivot. The model was restrained in roll by a wire from another cleat near one wing tip leading to an auxiliary weighbeam above the tunnel. The rig was stabilized by the usual wires to weights in oil pots below the working section. The rear position of the centre of rotation in incidence made necessary the off-axis position of the model rig mentioned above, since otherwise the model would have been too low in the section at high incidences.

This rearward position of the centre of rotation in incidence also raised complications with the ground represented, since the ground height to the c.g. varied through the incidence range. Four ground-board positions were used in the tunnel and data at constant ground height was subsequently produced by cross-plotting. The holes in the ground board were kept as small as practicable but although no allowance for movement of the wires in yaw was necessary (the ground board having a turntable), the hole size needed to allow for blow-back and the movement with incidence was not insignificant and a little interference on the model may have occurred. A rear flap on the ground board was adjusted before each test run with the model at a medium incidence in order to keep the velocity on both sides of the ground board equal.

For measurement of elevon hinge moment, a short sting was fixed to the control on one side and a wire passed to a small capstan on an auxiliary weighbeam above the tunnel. A weight wire was used here also, but in spite of reasonable care being taken with this wire rig, the wind speed had to be reduced for these tests to avoid control buffet.

4. *Range of Tests.*

With a few exceptions noted later, the wind speed for these tests was 250 ft/sec, i.e. at a Reynolds number based on root chord of $7{\cdot}86 \times 10^6$.

Measurements of lift, longitudinal and lateral stability were made over the range of wing incidence, -2 deg to 20 deg, and sideslip, -2 deg to $+10$ deg, with the elevons set as elevators at angles of 0, -5, -10, -15 and -20 deg. For these tests the model was in the 'flight' condition shown in Fig. 1 and described in Section 2, but no control tabs were represented. However, a series of secondary check tests were made with a typical setting of the outer geared tabs of $+8$ deg, and with the flow through the engine duct both increased and decreased from normal (equivalent to engine idling conditions in flight). Also checks were made on the effect of representing the retracted air brakes, and sealing the elevon hinge gap (since the gap flow would be sensitive to Reynolds number). Some tests were also made with the undercarriage removed. A longitudinal run was repeated at $V = 50$, 100 and 200 ft/sec in addition to the normal speed of 250 ft/sec to check scale effect (giving a complete range of Reynolds number based on root chord of $1{\cdot}57$ to $7{\cdot}86 \times 10^6$).

A limited amount of this basic test programme was repeated with the ground board in the tunnel, the lateral measurements being restricted to a few incidence runs at sideslip angles of 2 and 4 deg. Four ground-board positions were used, and data at c.g. heights of $0{\cdot}147\ c_0$ and $0{\cdot}285\ c_0$ was found from subsequent cross-plots. The value of $h/c_0 = 0{\cdot}147$ corresponds to the case where the main wheels are almost touching the ground.

With the elevons deflected differentially, aileron power was measured over the incidence range 0 to $+20$ deg. Differential deflections of ± 5, ± 10 and ± 15 deg were superimposed on normal 'elevator' deflections of $\eta = 0$, -5, -10 and -15 deg up to a limit on the total angle of 25 deg. Rudder deflections of $+5$, -10, -20 and -30 deg were also tested with elevator settings of $\eta = 0$, -5, -10 and -15 deg since it was considered likely that some aerodynamic interference might occur. The hinge-moments on the elevon were measured every 5 deg in a range of control angle from -20 to $+20$ deg over the incidence range 0 to $+20$ deg. However, control buffeting occurred at one or two extreme negative control angles at low incidence in spite of a lower wind speed of 200 ft/sec being used for these hinge-moment tests, and the results at these conditions were not reliable.

A few surface oil and smoke studies were made on this model, but the quality of the photographs was too poor for reproduction in this Report. Reference will be made to these, however, in Section 7.

5. *Corrections.*

Conventional blockage corrections have been applied to these wind-tunnel results, the wake blockage corrections of Ref. 2 being included.

The following constraint corrections of Ref. 3 have also been applied to incidence and drag:

$$\Delta\alpha = 0{\cdot}382\, C_L$$

$$\Delta C_D = 0{\cdot}00666\, C_L{}^2$$

For the tests with ground, no constraint corrections have been used, since these were negligible compared with effect of the ground itself. For the hinge-moment tests no overall forces were measured, but corrections to incidence from similar previous test conditions have been applied.

6. *Presentation of Results.*

All the data given in this note have been presented with reference to stability-axes, and unless stated otherwise the moment reference point is at $0{\cdot}558\, c_0$ along the wing root chord. The data from the flight tests, however, were quoted about the c.g. at $0{\cdot}548\, c_0$, so where comparisons have been made the tunnel results have been transferred to this origin.

The derivatives quoted in this Report have been obtained graphically from plots at a large scale, and although the longitudinal and lateral stability derivatives raised no particular problems, the comparatively small number of measured points made the control derivatives more difficult to determine, and consequently not so reliable. The curves of C_Y and C_n against sideslip were not by any means linear at small angles and both y_v and n_v were particularly sensitive to the range of sideslip used. For the main body of the data a sideslip range of ± 2 deg has been used, but for comparison with flight data the lateral derivatives were found for the sideslip range of 0 to 5 deg, since this was the order of the range used in the 'steady sideslip' flight tests.

In the figures, the main data from longitudinal tests are presented in Figs. 2 to 10, and from lateral tests in Figs. 11 to 15. The results of the secondary tests mentioned in Section 4 are shown in Figs. 16 to 24 and the effects of ground in Figs. 25 to 29. The control derivatives and hinge-moments are given in Figs. 30 to 43 and, finally, tunnel-flight comparisons are shown in Figs. 44 to 48. Some smoke observations of the vortex breakdown position are given in Fig. 49.

7. *Results and Discussion.*

7.1. *Lift and Longitudinal Stability*, Figs. 2 to 10.

The basic lift-incidence curve in Fig. 2 shows that the non-linear lift due to the formation of leading-edge vortices appears at very small incidence and continues to grow throughout the incidence range. At high negative elevator angles this non-linear lift starts later in the incidence range and falls off at the highest incidences. The pitching-moment curves, Fig. 3, show that the growth of non-linear lift causes a small increase in stability at first with the elevator set at zero. The C_m*vs.* C_L curve is reasonably smooth and regular however, but at the higher negative settings reversed non-linear lift is developed over the outer portions of the controls at small incidences, and at high incidence the interruption of the leading edge at the control hinge has an adverse effect on the loading of the tip. The total effect of deflecting the elevator upwards is thus to make the C_m*vs.* C_L curves progressively more non-linear with a tendency to pitch up a little at high lift coefficients. The change of lift and pitching moment with elevator movement increases slightly with incidence as may be seen in Figs. 4 and 5 and in the plots of $\frac{\partial C_L}{\partial \eta}$ and $\frac{\partial C_m}{\partial \eta}$ in Fig.

6. As might be expected from the above discussion, the derivative $\frac{\partial C_m}{\partial \eta}$ is reduced at negative elevator settings, this reduction being about 20 per cent at the higher incidences. The trimmed values of elevator setting are also shown in Fig. 4 for both the moment reference point of the tunnel tests and the c.g. of the flight tests (0·558 c_0 and 0·548 c_0 respectively). The position of the aerodynamic centre with reference to the centreline chord of the wing is shown in Fig. 7 for elevator settings of zero and -20 deg. As incidence increases there is a slow forward movement at $\eta = 0$ from 62 c_0 to 58 per cent c_0 after an initial rearward movement from 60 per cent c_0 near zero incidence. However, the more non-linear nature of the pitching-moment curves at negative elevator setting is reflected in the greater forward movement shown at $\eta = 20$ deg.

Drag polars are shown in Fig. 8 over the range of elevator settings, and selected plots of C_D *vs.* C_L^2 and induced drag factor in Figs. 9 and 10 respectively. There is a large increase with elevator movement of both C_{D_o} and induced-drag factor as might be expected but this is most marked at low lift coefficients.

7.2. *Sideslip Tests*, Figs. 11 to 15.

The variation with sideslip of C_Y and C_n is shown in Figs. 11 and 12 respectively, and it will be noted that there is a tendency for inflexions to appear in these curves at the origin which is not so apparent in the similar curves of C_l shown in Fig. 13. The main contribution to the yawing moment at angles of sideslip is of course from the fin, and this non-linearity at small angles probably indicates the presence of vortices shed from the body and nacelle passing near the fin rather than any specific interference from the wing vortex field. The effect of elevator movement is regular and progressive on these curves, and this is also apparent from the derivatives n_v, y_v and l_v plotted in Fig. 15. A sideslip range of -2 deg $< \beta < +2$ deg has been used for these derivatives and it should be noted that because of the inflexion in the curves near the origin, n_v's of about half the value of those plotted would have been obtained had the sideslip range -1 deg $< \beta < +1$ deg been used. Directional stability rises steadily with lift coefficient to reach almost double the initial value at the highest C_L. At constant incidence there was a strong destabilizing effect of up-elevator movement on yawing moments, and although this was probably due to interference on the flow field at the base of the fin, this could not be confirmed since tests without fin were not possible. The effect of sideslip on pitching moments is very small, as may be seen in Fig. 14.

In the basic plots of C_Y, C_n and C_l, Figs. 11 to 13, some slight asymmetries are noticeable in yaw. These are thought to be due to small imperfections in the model and rig rather than inherent asymmetries of the flow field.

7.3. *Miscellaneous Tests*, Figs. 16 to 24.

The scale effect on lift and pitching moment for a range of wind speed $50 < V < 250$ ft/sec is shown in Figs. 16 and 17 respectively. Little effect can be seen in this range above $V = 100$ ft/sec, but at the lowest speed of $V = 50$ ft/sec higher lift coefficients were obtained associated with a small nose up pitching-moment increment and may well have been due to more lift being developed on the body nose in conditions of laminar flow. The undercarriage appeared to cause only small effects on pitching moment, Fig. 18, and rolling and yawing moments, Figs. 21 and 23, but there is some evidence of some interference on elevator power. In Figs. 19, 21 and 23 the effect of sealing the elevon hinge gap on these same components is shown, and it will be seen that there is a considerable effect on longitudinal stability. The flow through the hinge gaps, which were carefully scaled from the aircraft geometry, would have been sensitive to Reynolds number, and it is hardly surprising that a significant difference was found between tunnel and flight as regards the elevator angles to trim (*see* section 7.6). Blocking the intake flow, Figs. 20, 22 and 24, seemed to have no noticeable effect. By means of modifications to the nacelle exit, the duct flow was increased approximately by 50 per cent and this also had no effect (not shown).

The elevon tab arrangements on the aircraft were complicated since inboard spring tabs were used in conjunction with outboard geared tabs, the latter also being used as trimmers (Ref. 1). To check the import-

ance of not representing tabs on the model, outer tabs at a fixed anti-balance angle of 8 deg were fitted to the elevons which were set as elevators at $\eta = -20$ deg. Little effect of these tabs was in fact found, the most significant effects being on laterals, and these are shown in Figs. 22 and 24.

7.4 *Ground Effect*, Figs. 25 to 29.

The ground effect on lift, Fig. 25, shows the expected small loss of lift at low incidence and the substantial gain at high values. The lift increase at an incidence of 18 deg is about 30 per cent for the wheels-on-ground case of $\frac{h}{c_o} = 0{\cdot}147$, but this is reduced a little at up-elevator settings when the effective ground height is increased. The pitching-moment curves in Fig. 26 show the large stabilizing effects of ground proximity at high lift coefficients and the slight nose-up C_{m_o} increment at low incidence. At a constant incidence of 18 deg there was an increase in elevator power of about 14 per cent due to ground $\left(\frac{h}{c_0} = 0{\cdot}147\right)$. The effect of ground on the drag polars is shown in Fig. 27 and on laterals in Figs. 28 and 29. There is a tendency for both $-l_v$ and n_v to increase with ground present, but only at the higher incidences.

7.5. *Control Power and Hinge Moments*, Figs. 30 to 43.

The basic variations of C_Y, C_n and C_l with rudder deflection are shown in Figs. 30 to 32 and with aileron deflection in Figs. 36 to 38. As with the plots against sideslip (Figs. 11 to 13), some asymmetry is apparent in the model and rig, particularly as regards sideforce and rolling moment at small elevator settings, and some scatter is noticeable in the smaller quantities measured (e.g. sideforce). However, all these curves are remarkably linear and free from kinks, and the plotted control-power derivatives in Figs. 33 to 35 and 39 to 41 show little of interest except perhaps that $-l_\xi$ drops sharply when the combination of elevator and aileron setting dictates an elevon angle in excess of 10 deg down or 20 deg up.

The hinge-moment results for the elevon in Figs. 42 and 43 show smooth variations with incidence at constant control setting and with control setting at constant incidence. There is a tendency for a non-linear increase in hinge moment to develop at the higher angles.

7.6. *Tunnel-flight Comparison*, Figs. 44 to 48.

In Fig. 44 the comparison between the flight and tunnel C_L *vs.* α curves is shown to be excellent, except for a small discrepancy at the top end of the incidence range thought to be due to the difficulties of applying position-error correction at very low speeds in flight. However, the comparison of elevator angle to trim in Fig. 45 is not so good although the variation with C_L is similar. It was noted in Section 7.3 that there was considerable effect on pitching moments of flow through the elevon gap and that this would be sensitive to scale.

The comparison of sideslip derivatives is shown in Fig. 46, the only flight results shown being those obtained by the 'steady sideslip' technique. This technique requires the use of control derivatives in the analysis and it will be seen that good agreement in n_v between the flight and tunnel data is obtained when flight values of n_ξ and n_ζ are used in preference to the tunnel values. Figs. 47 and 48 show that this effect arises mainly from the flight-tunnel differences in n_ζ since there was fair agreement in the values of n_ξ at some C_L's. However, the flight-tunnel comparison of l_v was good and that of y_v fair except at high C_L's.

The comparison of aileron derivatives in Fig. 47 shows well defined differences in n_ξ and l_ξ which reflect both the possibilities of scale-effect on the hinge-gap flow and aero-elastic distortion in flight at high speeds (low C_L's), but the consistent difference in the rudder derivatives, n_ζ, shown in Fig. 48 is more difficult to account for. These rudder derivatives were obtained from the transient response to a rudder pulse in flight, and the mean line through rather scattered points has been drawn for the purposes of this comparison. On the face of it, this discrepancy in n_ζ seems likely to be due to genuine scale effect or due to comparing oscillatory with static data, but further 'static' measurements in flight may help to resolve this.

7.7. *Vortex Breakdown.*

At high combinations of incidence and sideslip the vortex breakdown position was observed on the model by means of smoke, and this is plotted in Fig. 49. Some preliminary experiments with smoke have also been made in flight and the approximate position of the breakdown observed from another aircraft has been included in this figure. Within the usual limitations of this type of observation, no gross scale effect between tunnel and flight data is apparent. The slight tendency for a more upstream vortex breakdown position in flight is thought to be due to the adverse effect of the elevon deflection required to trim, which was not represented on the model. Other unpublished tunnel work has indicated that discrepancies of this order (i.e. about $\Delta\alpha = 1$ deg) are likely in this case. Surface flow visualization studies showed very similar patterns in the tunnel and in flight.

8. *Conclusions.*

The main purpose of these wind-tunnel tests was to provide a basis for the flight-tunnel comparison of data and to give general wind-tunnel support for the flight research work on the aeroplane.

The longitudinal and lateral data were generally smooth and regular, but some complications arose with the use of large aerodynamically-balanced elevons on the wing. When deflected, the interruption in the wing leading edge was severe, due to the set back position of the hinge-line, and some non-linearities in the pitching-moment characteristics were attributed to this. At high negative elevator settings there was a 20 per cent reduction in elevator power and a strong de-stabilizing effect on n_v (at constant incidence), possibly due to local interference on the efficiency of the fin. The curves Cn *vs.* β showed inflexions at the origin, probably due to the influence of body-vortex field on the fin.

The flow through the elevon gap was also shown to be of some significance, particularly on pitching-moments, and the scale effect on this was thought to be a contributory cause of the flight-tunnel discrepancies in elevator-to-trim and the values of aileron derivatives. However, the effect of control deflection was in general progressive and regular except at extreme settings. There was a tendency for a non-linear increase of hinge moment to be developed on the elevon at the higher angles.

The interim tunnel-flight comparisons possible so far show a good measure of agreement for lift coefficients, sideslip derivatives and certain control derivatives, but significant differences are apparent in the values of the elevator angle to trim and the control-power derivatives. How far aeroelastic effects in flight and scale effects between flight and tunnel are responsible for these differences it is not yet known. Preliminary comparisons of tests made with smoke both in flight and in the tunnel have shown reasonable agreement in the position of vortex breakdown aft of the wing at high incidence.

TABLE I

Model Details

		$\frac{1}{8}$ *scale model*	*Aircraft*
Wing	gross area, S, sq ft	6·75	432·5
	span, b, ft	2·5	20
	root chord, c_o, ft	5·0	40
	thickness chord ratio, t/c	6%	6%
	section	Symmetrical, biconvex, circular-arc section	
	L.E. sweep	74° 42′	74° 42′
	T.E. sweep	0°	0°
	dihedral	0°	0°
	aerodynamic mean chord, $\bar{c}$, ft	3·8	30·4
	aspect ratio A, $(= {}^{b}/_{\bar{c}})$	0·66	0·66
Elevons	area (each) S_E, sq ft	0·533	34·1
	chord, c_E, ft	0·503	4·02
	chord aft of hinge, ft	0·333	2·66
	range of movement possible	±25°	+29° to −34°
	tab chord, in.	0·675	5·4
	tab span (outer pair only)	On each side	38% of control
	tab movement possible	8° used	12°
Fin	area external to fuselage, sq ft	0·489	31·3
	root chord, ft	0·911	7·29
	tip chord, ft	0·488	3·9
	L.E. sweep	60°	60°
Rudder	area, aft of hinge, sq ft	0·125	8
	range of movement (perp. to hingeline)	±30°	±36·5°
Moment reference point (C.G.)		0·558 c_o	0·548 c_o

LIST OF SYMBOLS

S Wing area, sq ft.

c_o Wing root chord, ft.

$\bar{c}$ Wing aerodynamic mean chord, ft

b Wing span, ft

$A = {}^{b}/_{\bar{c}}$ Wing aspect ratio

S_E Elevon area, sq/ft

c_E Elevon chord, ft

q Dynamic head, $\frac{1}{2}pV^2$, lb/sq ft

V Wind speed, ft/sec

Forces and moments in lb and lb ft units to stability axes

C_L = Lift/$\frac{1}{2}pV^2S$;

C_D = Drag/$\frac{1}{2}pV^2S$

C_Y = Sideforce/$\frac{1}{2}pV^2S$;

C_m = Pitching moment/$\frac{1}{2}pV^2S\bar{c}$

C_n = Yawing moment/$\frac{1}{2}pV^2Sb$;

C_l = Rolling moment/$\frac{1}{2}pV^2Sb$

C_H = Hinge moment/$\frac{1}{2}pV^2S_Ec_E$

α Incidence of wing, deg

β Sideslip of wing, deg (in radians when used in derivatives)

η Elevon angle, deg, used as elevator (in radians when used in derivatives)

ξ Elevon angle, deg, used as aileron (in radians when used in derivatives)

ζ Rudder angle, deg, (in radians when used in derivatives)

$$y_v = \frac{1}{2}\frac{\partial C_Y}{\partial \beta} ; \; y_\xi = \frac{1}{2}\frac{\partial C_Y}{\partial \xi} ; \; y_\zeta = \frac{1}{2}\frac{\partial C_Y}{\partial \zeta}$$

$$n_v = \frac{\partial C_n}{\partial \beta} ; \; n_\xi = \frac{\partial C_n}{\xi} ; \; n_\zeta = \frac{\partial C_n}{\partial \zeta}$$

$$l_v = \frac{\partial C_l}{\partial \beta} ; l_\xi = \frac{\partial C_l}{\partial \xi} ; l_\zeta = \frac{\partial C_l}{\partial \zeta}$$

Sign Conventions

α	Incidence, nose up, positive
β	Sideslip, nose to port, positive
η	Elevon used as elevator, down, positive
ξ	Elevon used as aileron, port up and starboard down, positive
ζ	Rudder angle, to port, positive
	Elevon tab, positive up at negative elevator angles (anti-balance).

REFERENCES

No.	*Author*	*Title, etc.*
1	P. L. Bisgood and C. O. O'Leary	Interim Report on low speed flight tests of a slender-wing research aircraft (Handley-Page HP.115). A.R.C. C.P. 838, November, 1963.
2	E. C. Maskell	A theory of the blockage effects on bluff bodies and stalled wings in a closed tunnel. A.R.C. R. & M. 3400, November, 1963.
3	H. Glauert	Wind-tunnel interference on wings, bodies and airscrews. A.R.C. Monograph, R. & M., 1566.

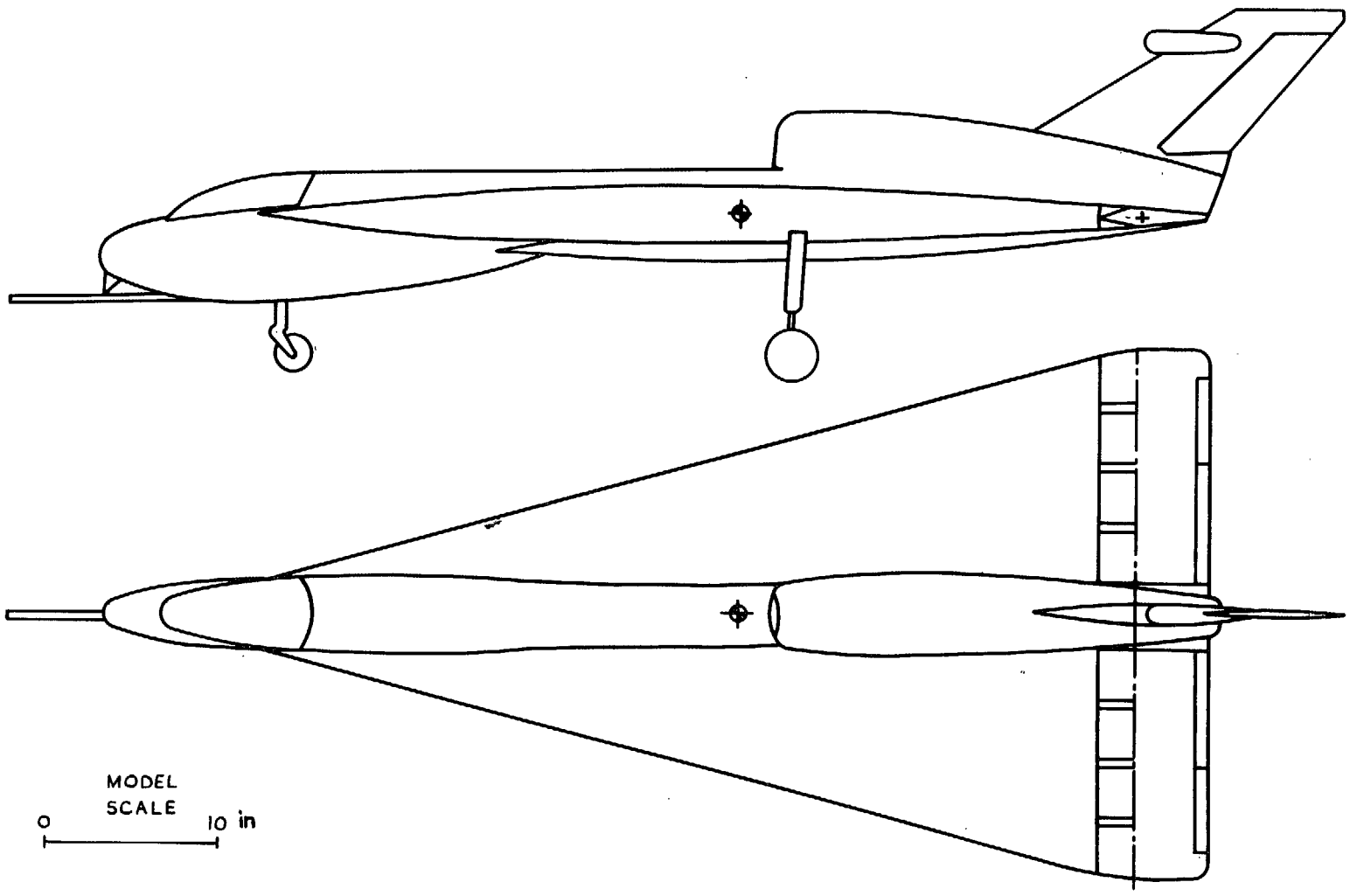

FIG. 1. General arrangement of HP115 model.

Fig.2

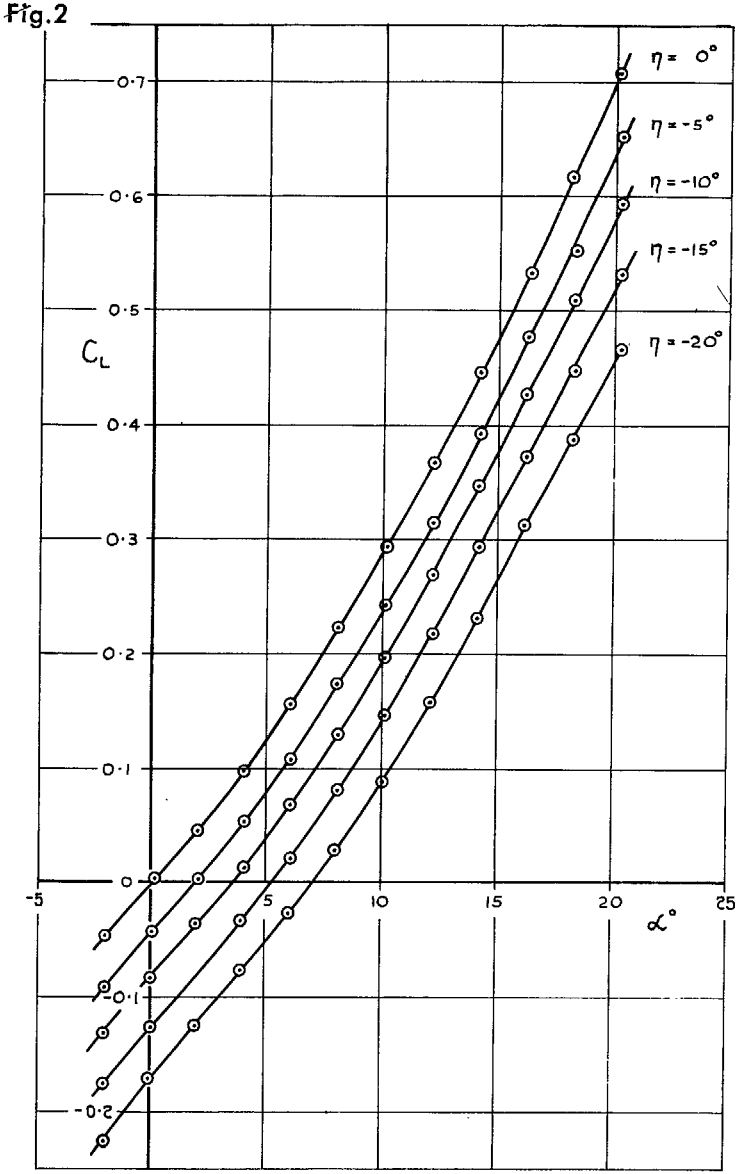

FIG. 2. Variation of Lift with incidence.

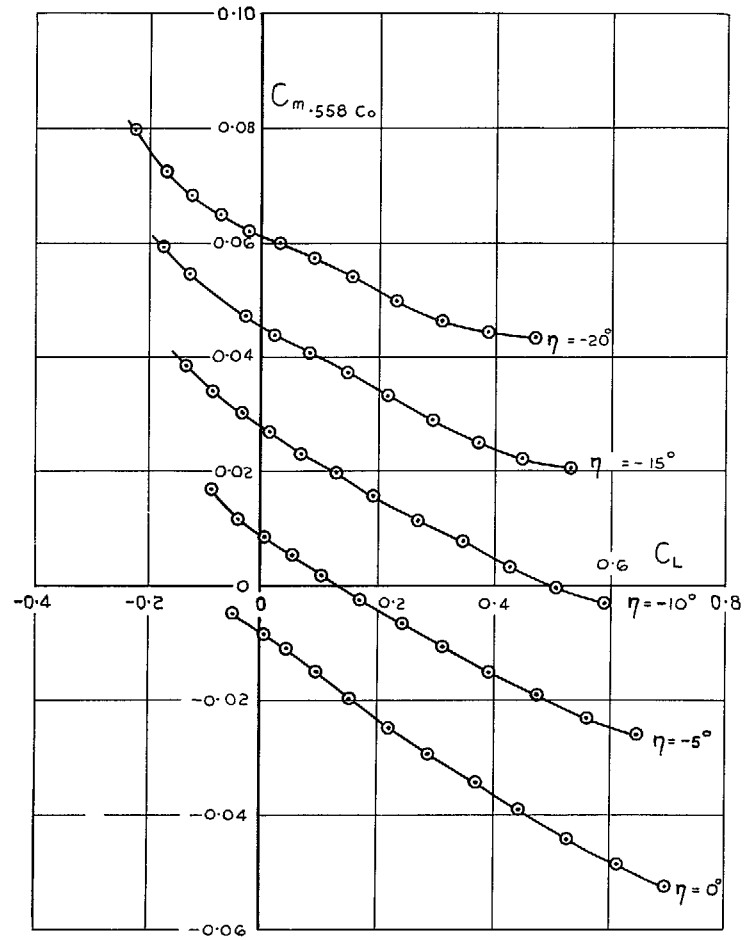

FIG. 3. Pitching-moment characteristics.

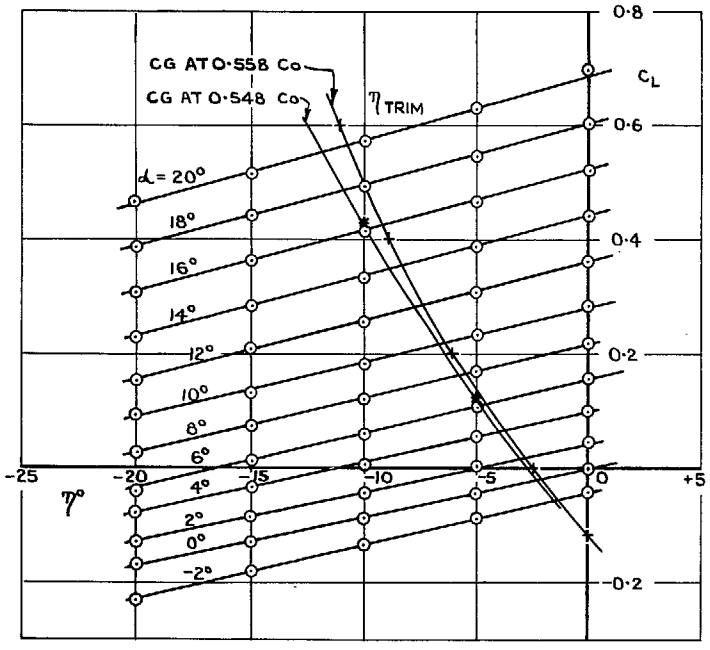

FIG. 4. C_L *vs.* η at constant incidence.

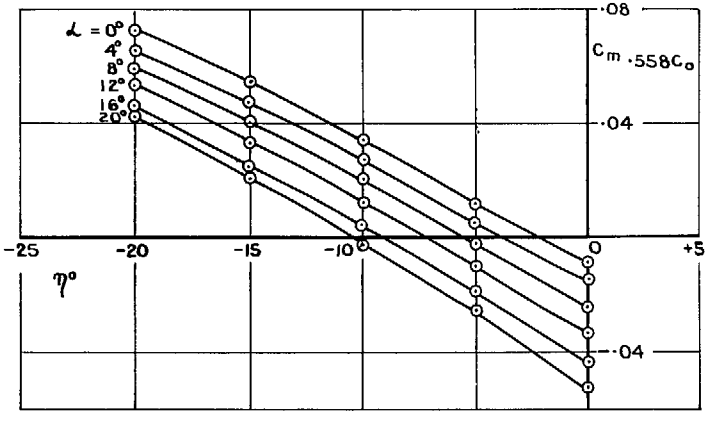

FIG. 5. C_m *vs.* η at constant incidence.

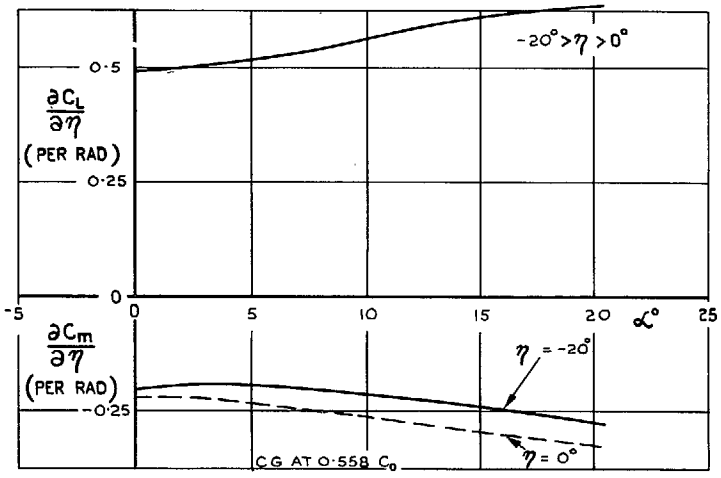

FIG. 6. Elevator derivatives $\partial C_L/\partial\eta$ and $\partial C_m/\partial\eta$.

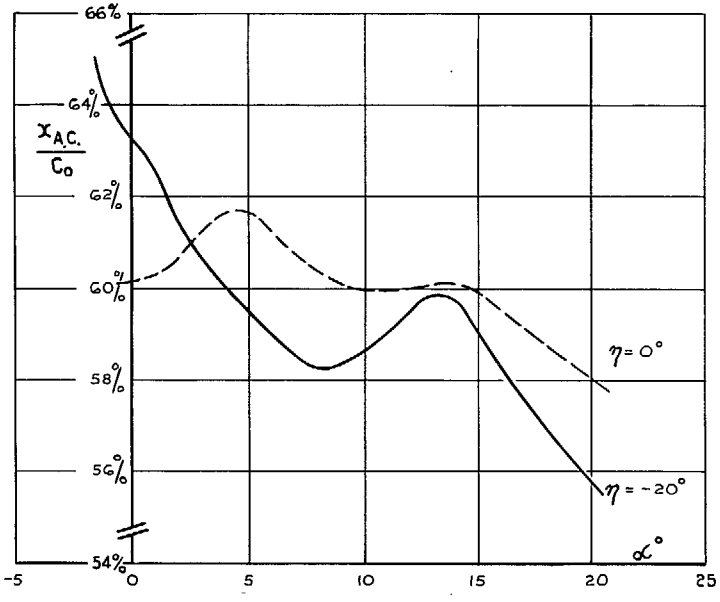

FIG. 7. Position of aerodynamic centre

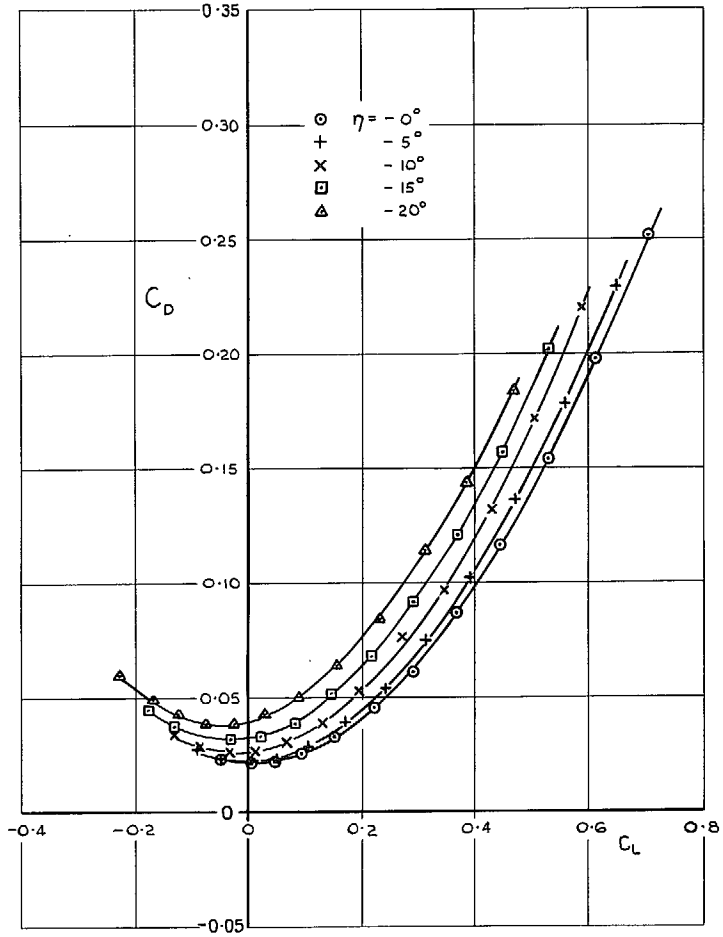

FIG. 8. C_D *vs.* C_L Curves.

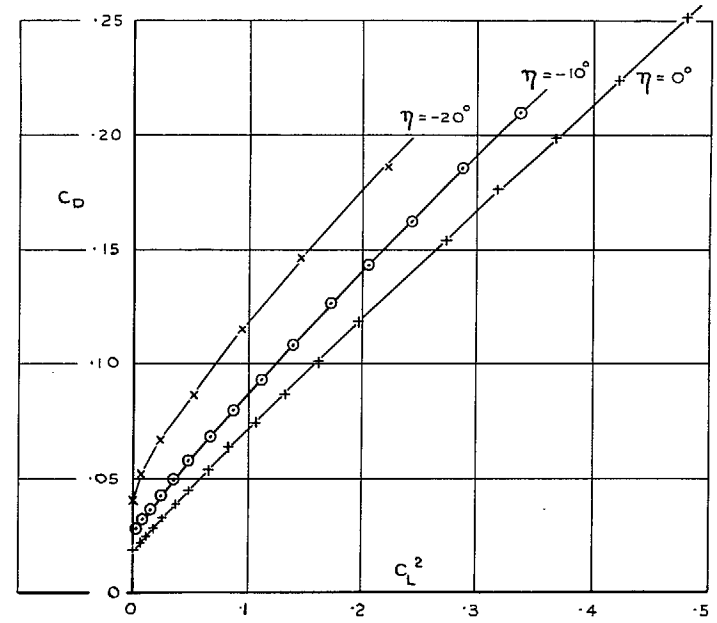

FIG. 9. C_D *vs* C_L^2.

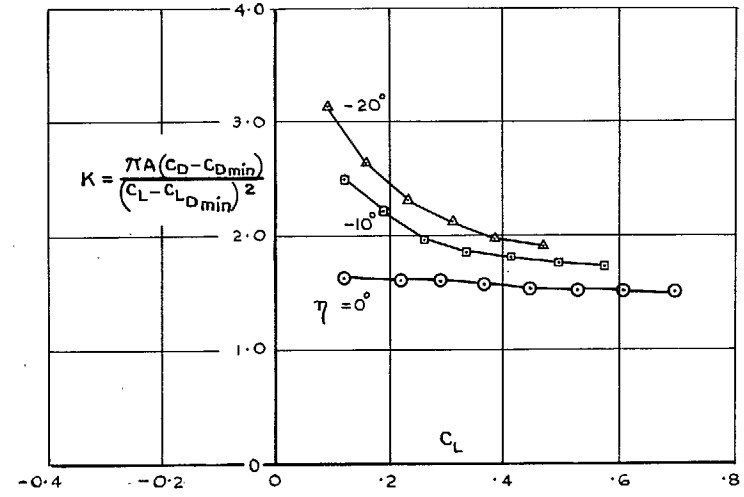

FIG. 10. Induced drag factor.

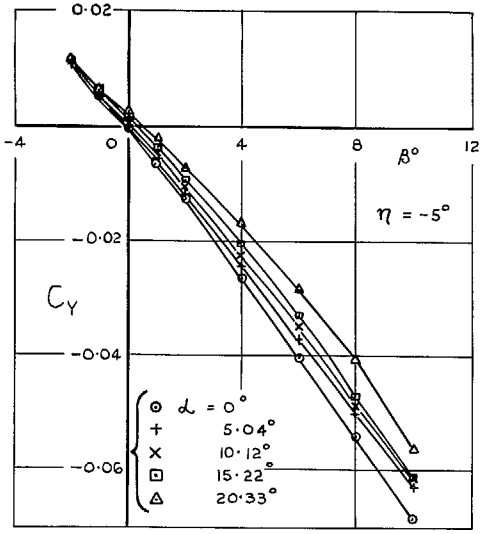

FIG. 11. $C_Y \sim \beta$.

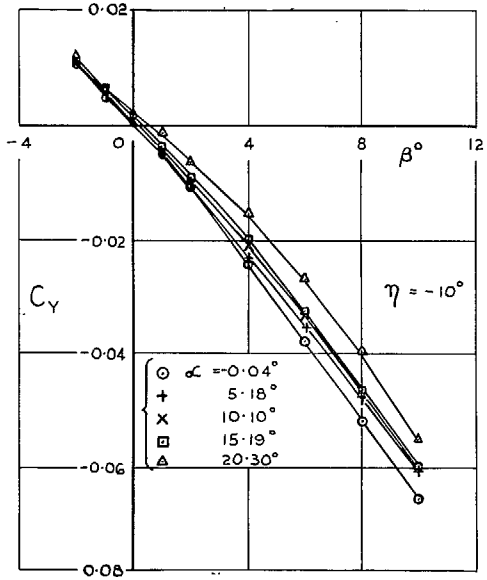

FIG. 11 (cont.). $C_Y \sim \beta$.

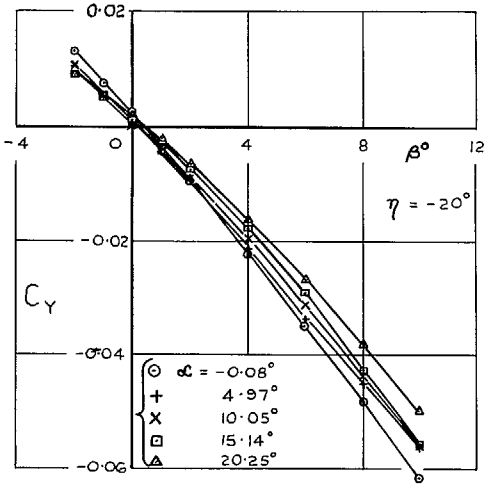

FIG. 11 (concl.). $C_Y \sim \beta$.

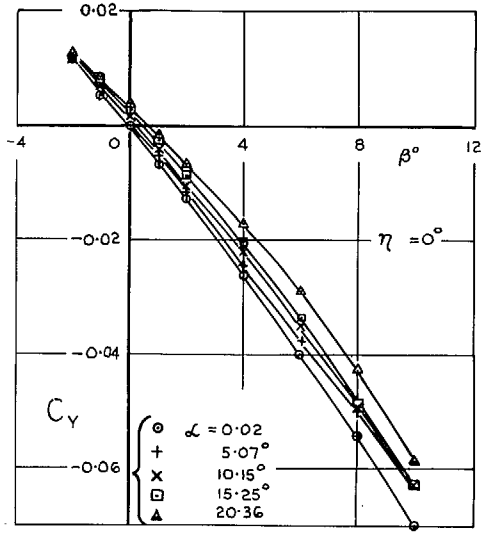

FIG. 11 (*cont.*). $C_Y \sim \beta$.

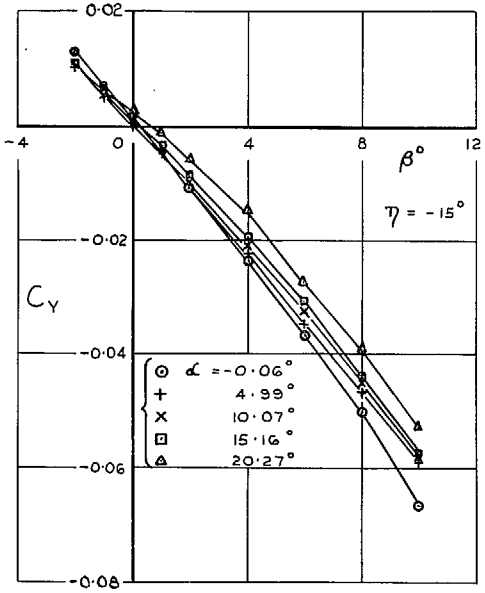

FIG. 11 (cont.). $C_Y \sim \beta$.

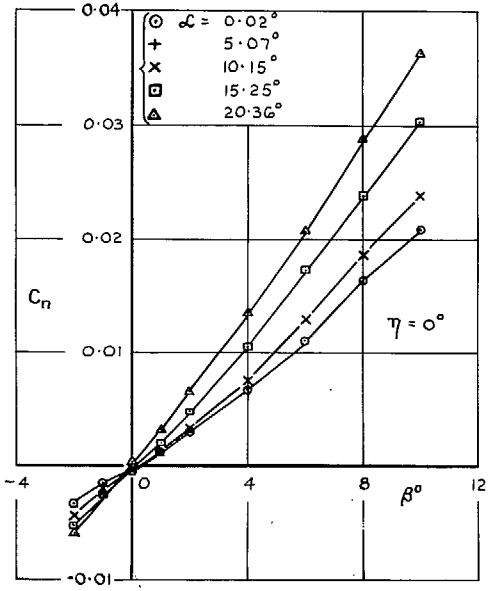

FIG. 12. $C_n \sim \beta$.

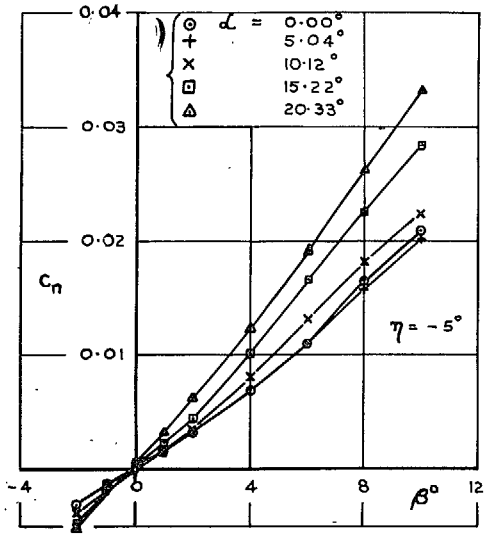

FIG. 12 (cont.). $C_n \sim \beta$.

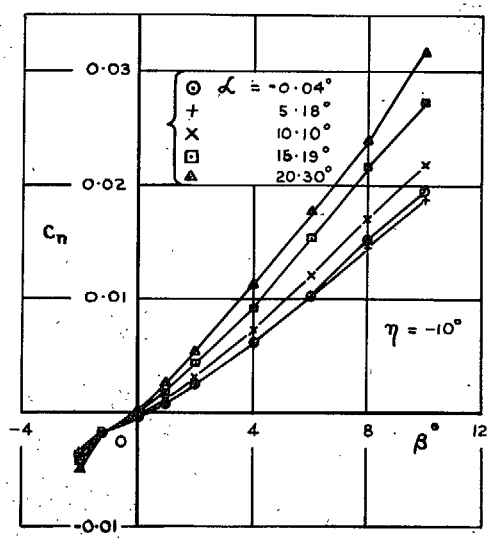

FIG. 12 (cont.). $C_n \sim \beta$.

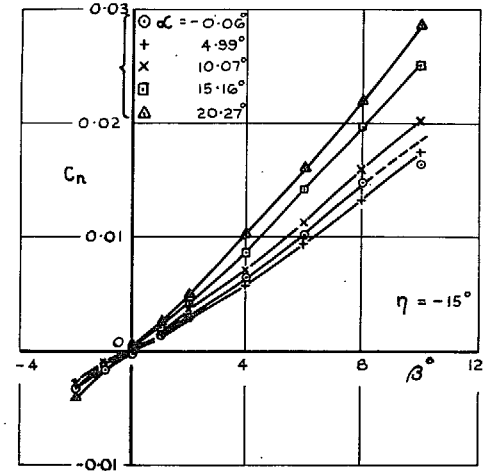

FIG. 12 (cont.). $C_n \sim \beta$.

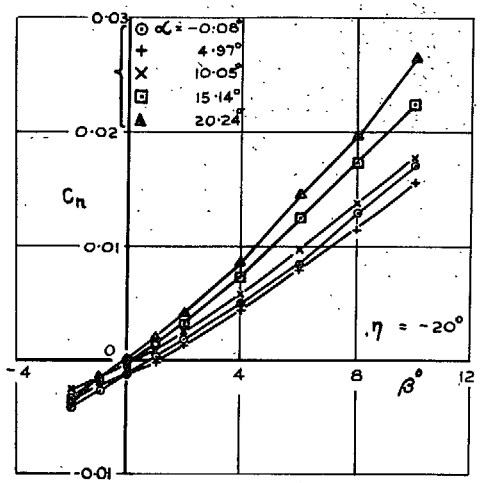

FIG. 12 (concl.). $C_n \sim \beta$.

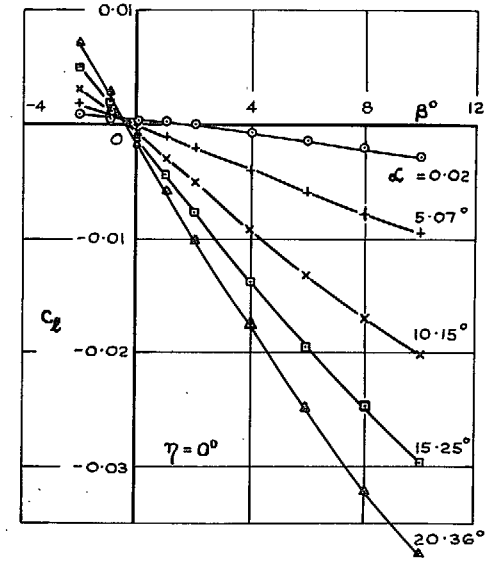

FIG. 13. $C_l \sim \beta$.

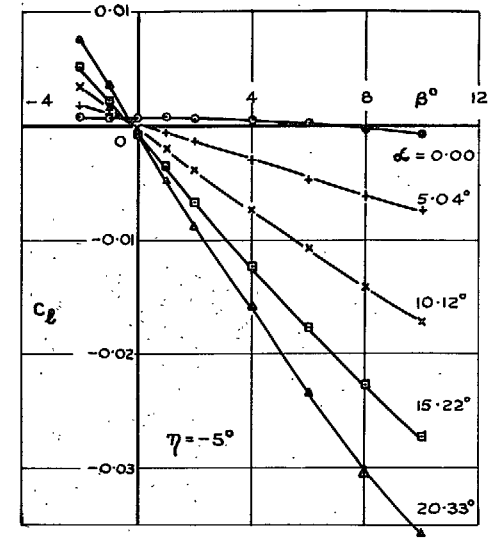

FIG. 13 (cont.). $C_l \sim \beta$.

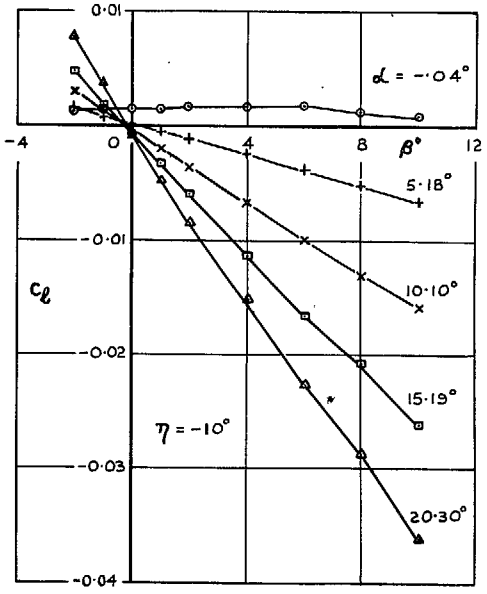

FIG. 13 (cont.). $C_l \sim \beta$.

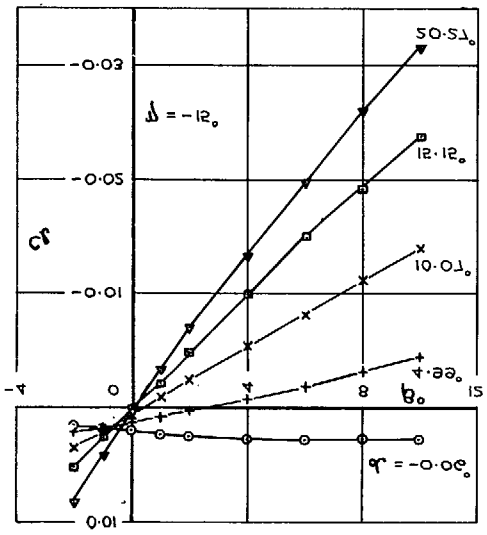

FIG. 13 (cont.). $C_l \sim \beta$.

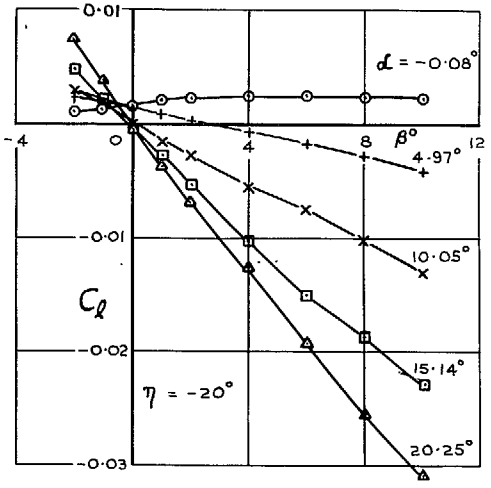

FIG. 13 (concl.). $C_l \sim \beta$.

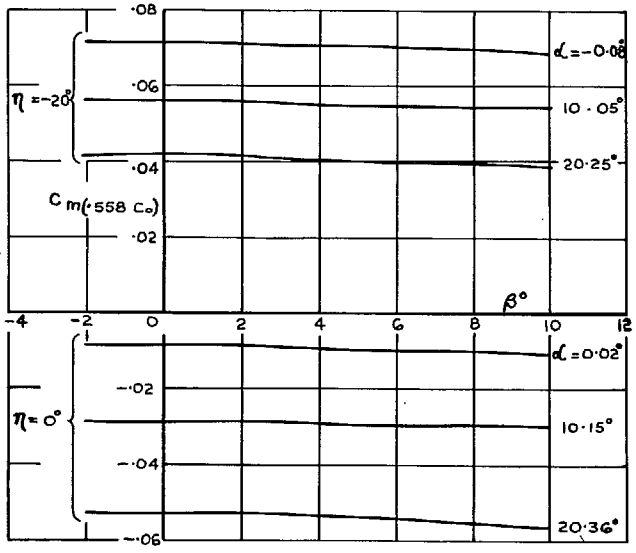

FIG. 14. Variation of C_m with sideslip.

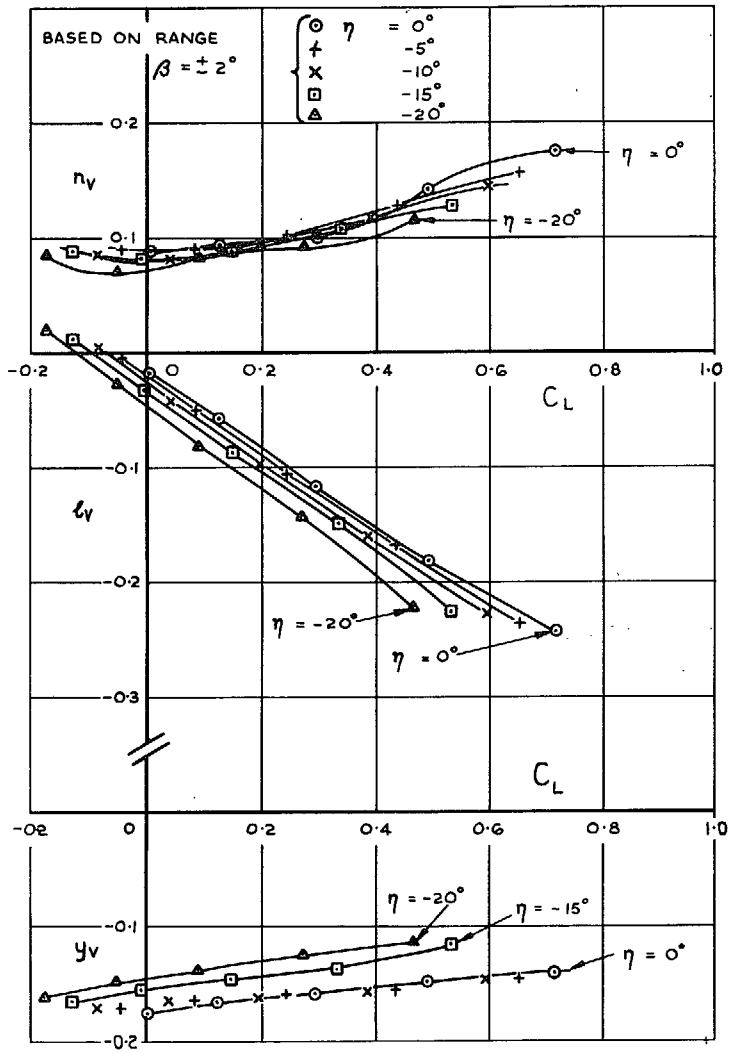

FIG. 15. Sideslip derivatives, n_v, l_v and y_v.

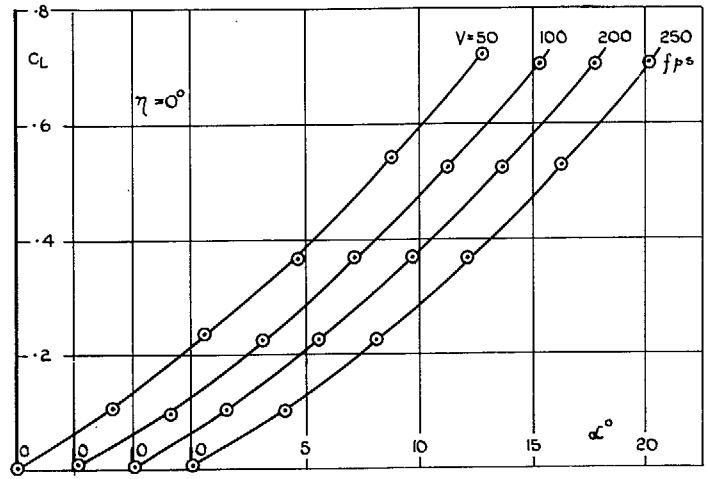

FIG. 16. Effect of scale on lift coefficients.

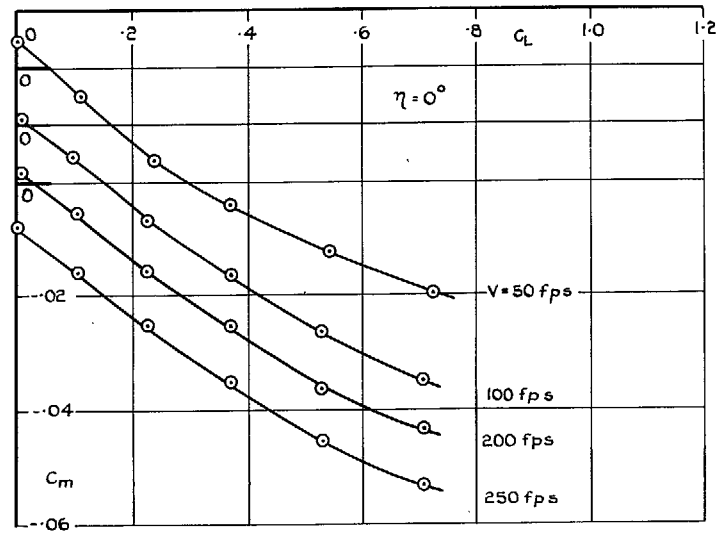

FIG. 17. Effect of scale on pitching moments.

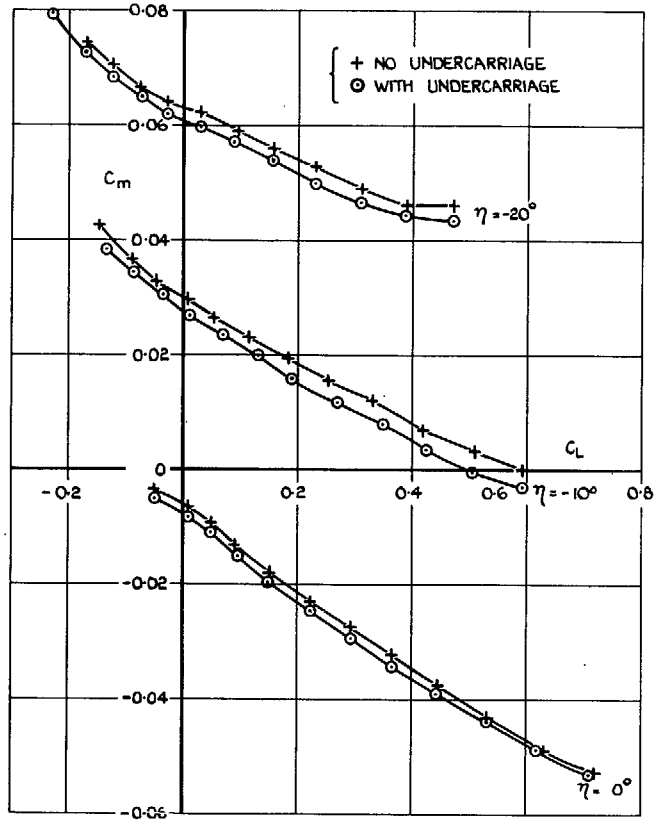

FIG. 18. Effect of undercarriage on C_m *vs.* C_L.

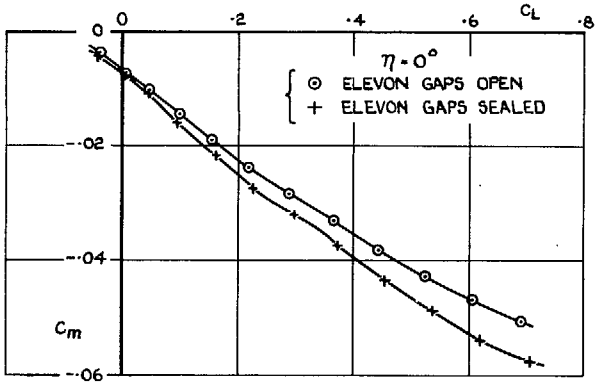

FIG. 19. Effect of sealing elevon gap on C_m *vs* C_L.

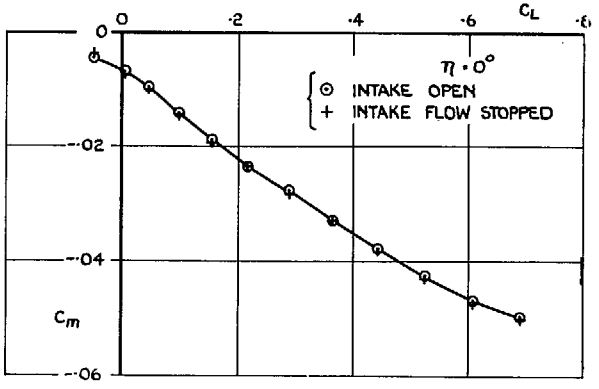

FIG. 20. Effect of blocking intake flow on C_m *vs.* C_L.

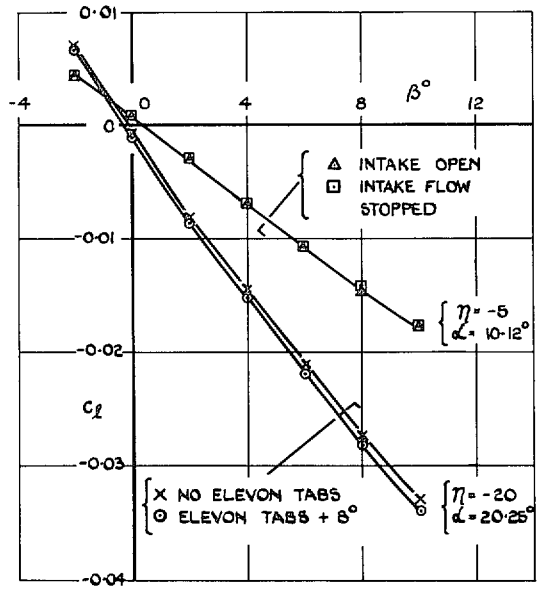

FIG. 21. Effect of sealing elevon gap and adding undercarriage on rolling moments.

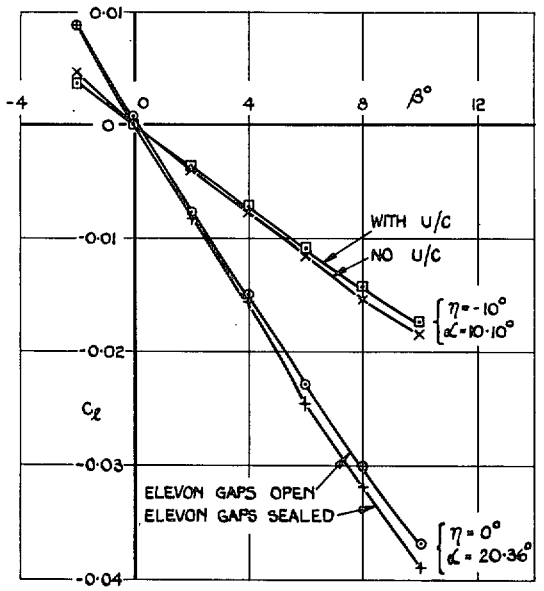

FIG. 22. Effect of blocking intake flow and deflecting elevon tabs on rolling moments.

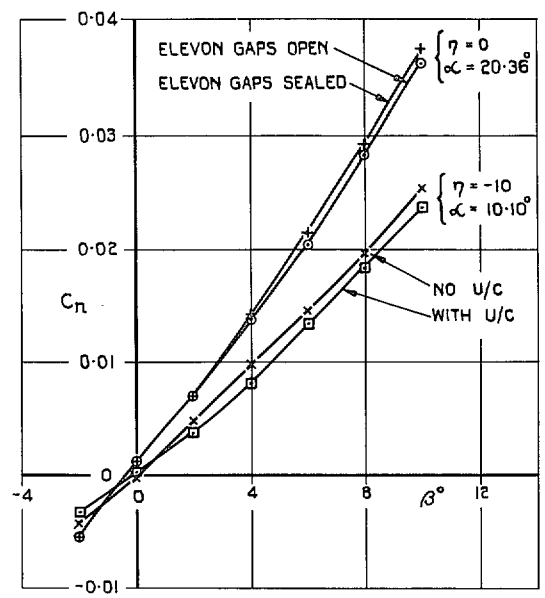

FIG. 23. Effect of sealing elevon gap and adding undercarriage on yawing moments.

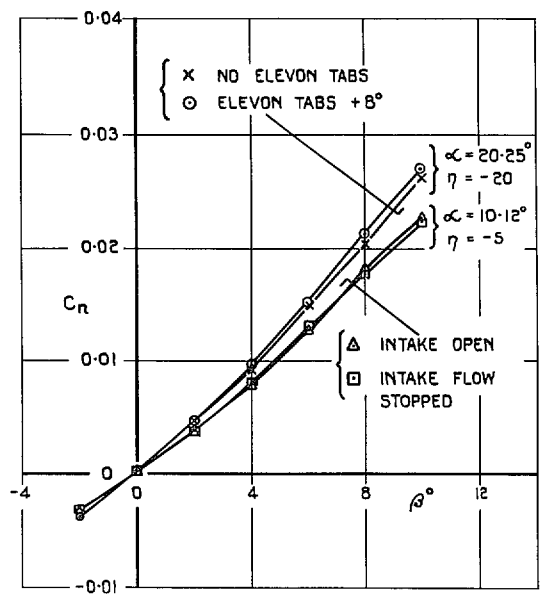

FIG. 24. Effect of blocking intake flow and deflecting elevon tabs on yawing moments.

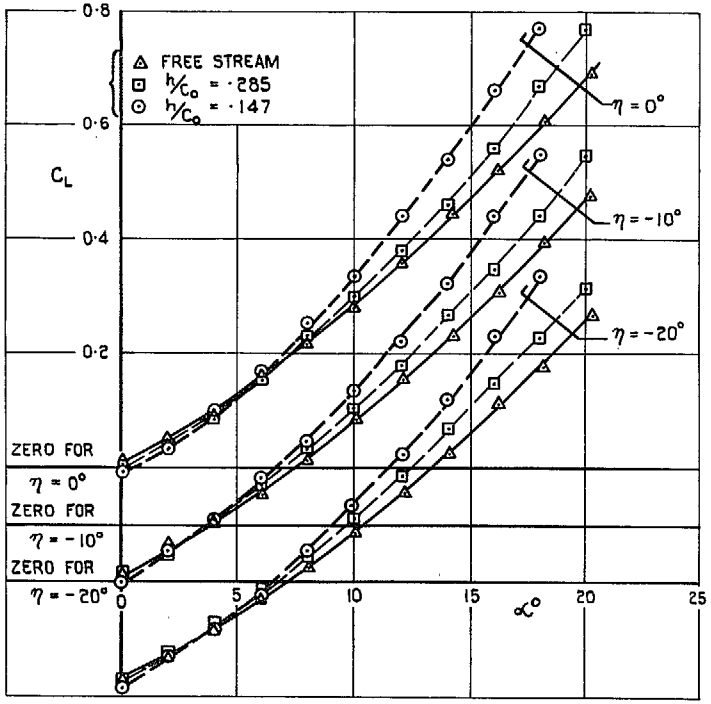

FIG. 25. Effect of ground on lift coefficients.

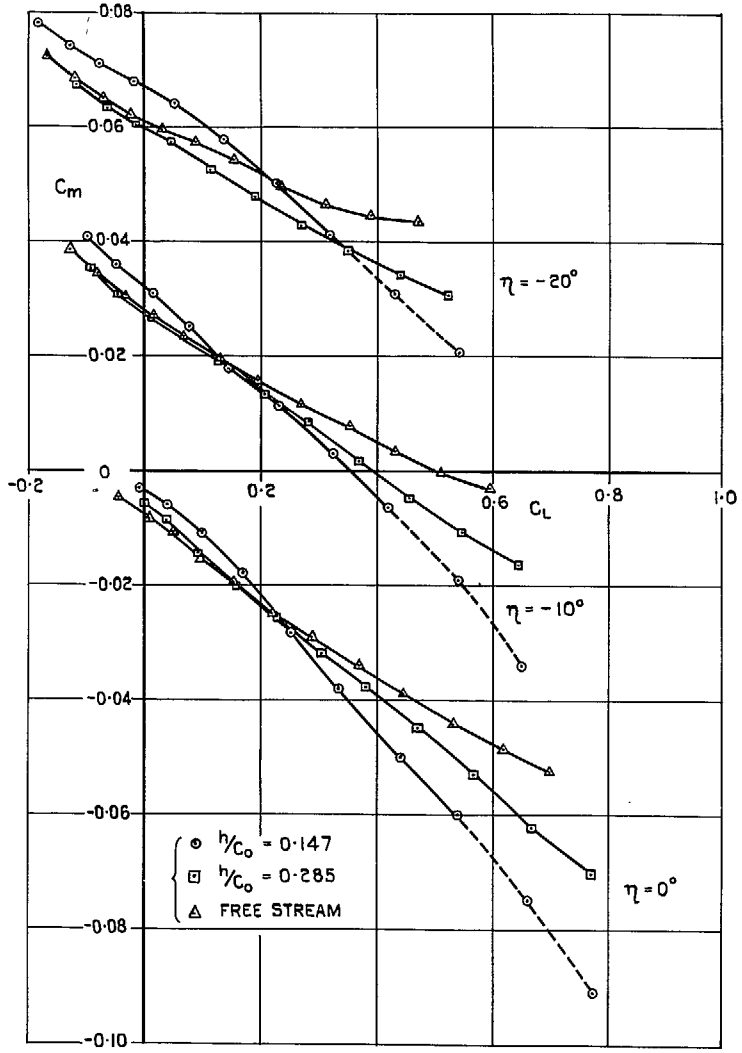

FIG. 26. Effect of ground on pitching moments.

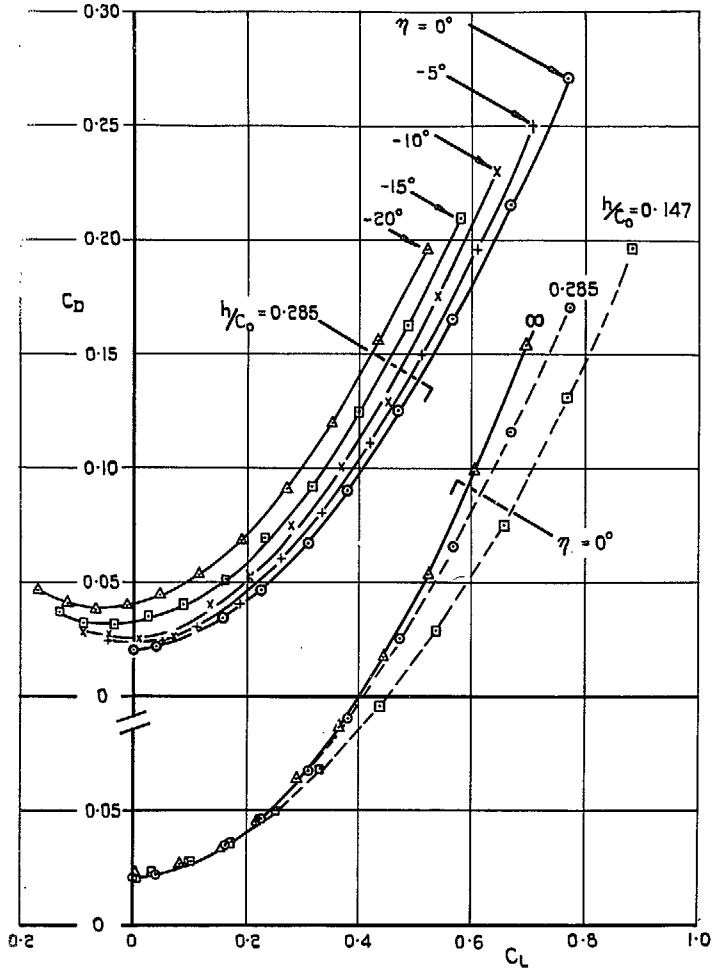

FIG. 27. Effect of ground on drag coefficients.

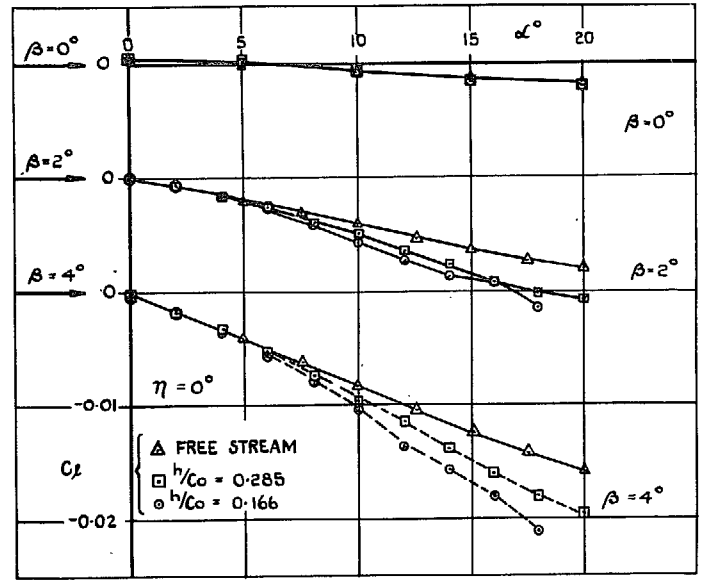

FIG. 28. Effect of ground on rolling moments.

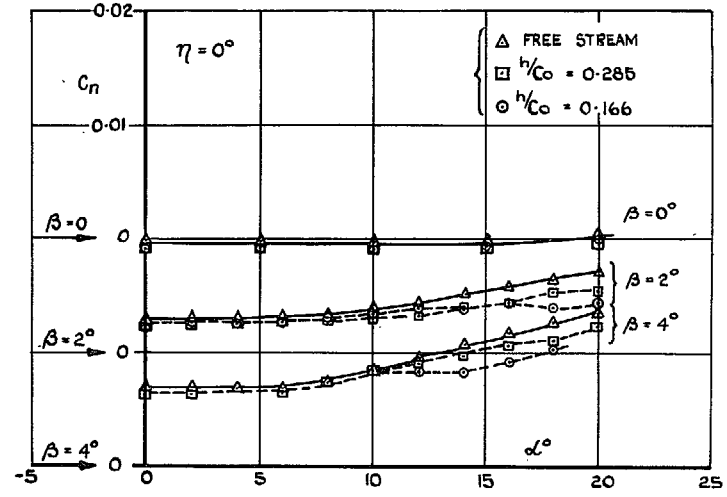

FIG. 29. Effect of ground on yawing moments.

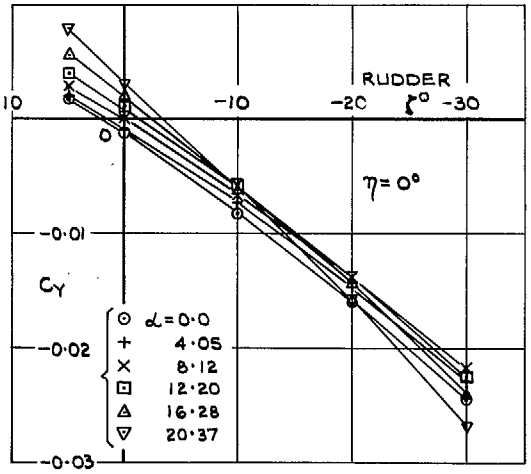

FIG. 30. $Cy \sim \zeta$.

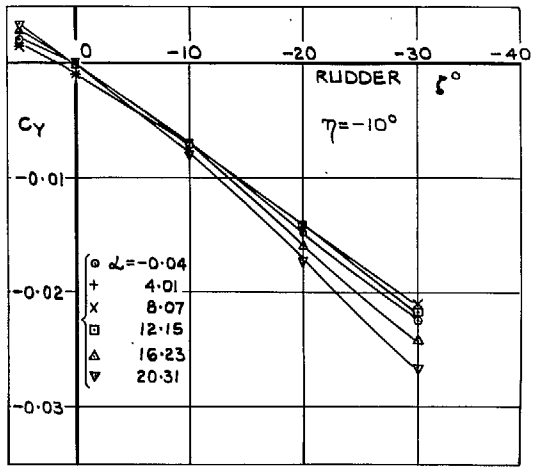

FIG. 30 (cont.). $Cy \sim \zeta°$.

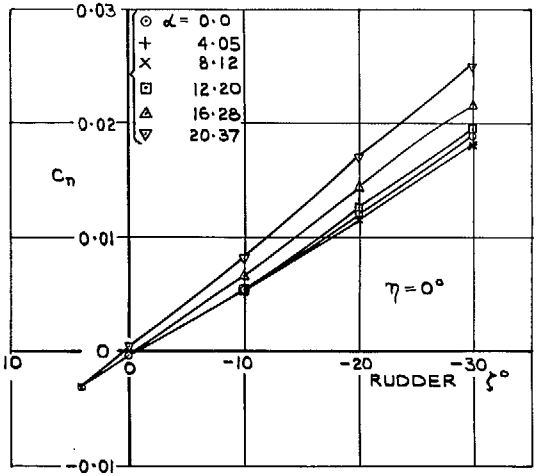

FIG. 31. $C_n \sim \zeta$.

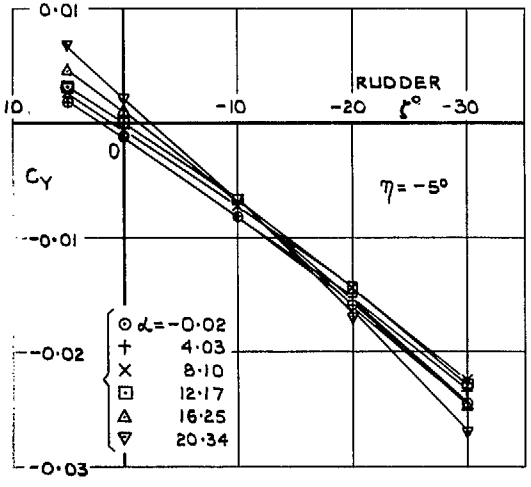

FIG. 30 (cont.). $Cy \sim \zeta$.

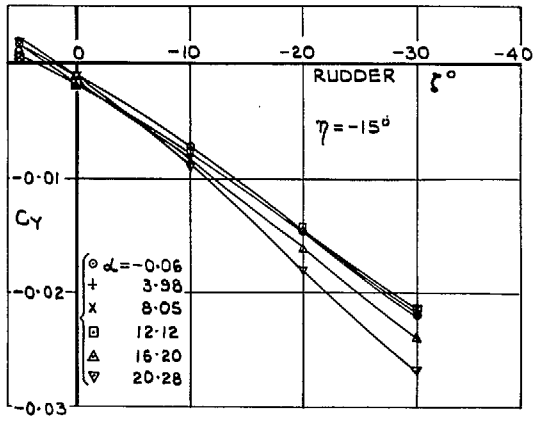

FIG. 30 (concl.). $C_y \sim \zeta$.

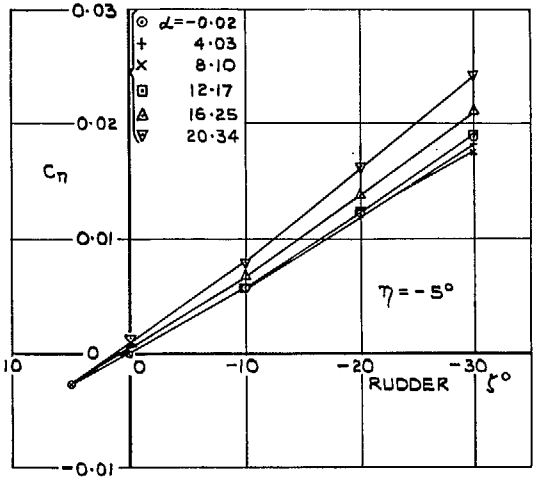

FIG. 31 (cont.). $C_n \sim \zeta$.

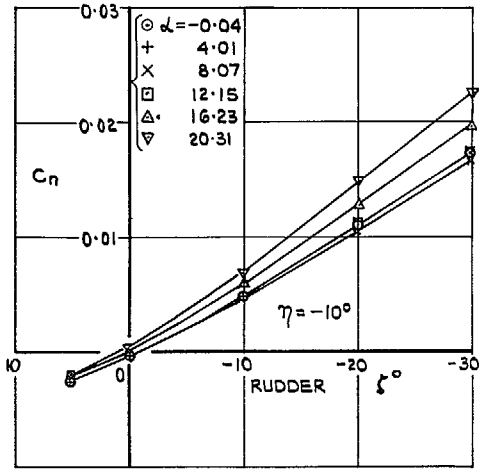

FIG. 31 (concl.). $C_n \sim \zeta$.

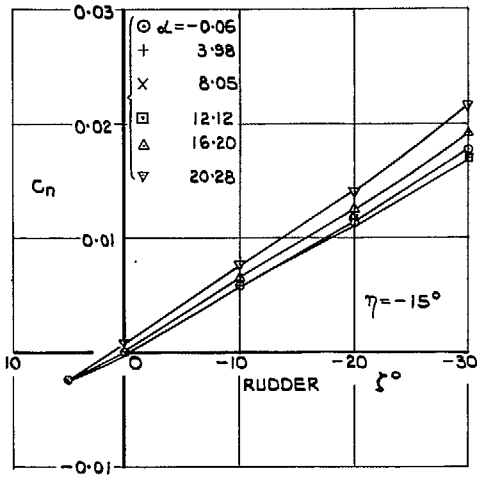

FIG. 31 (contd.). $C_n \sim \zeta$.

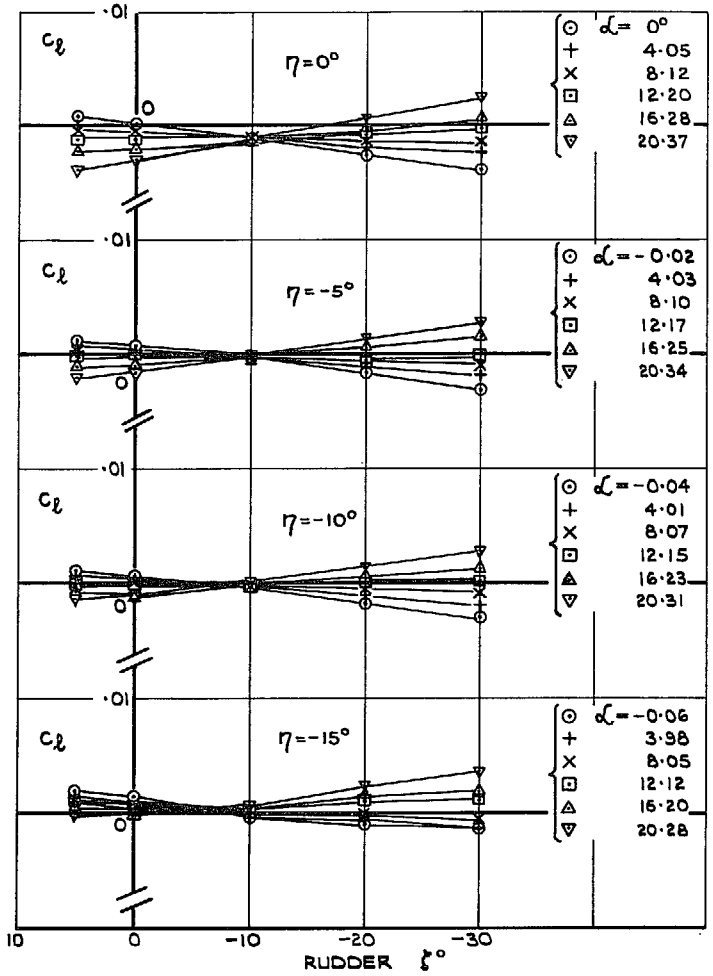

FIG. 32. C_l *vs.* ζ.

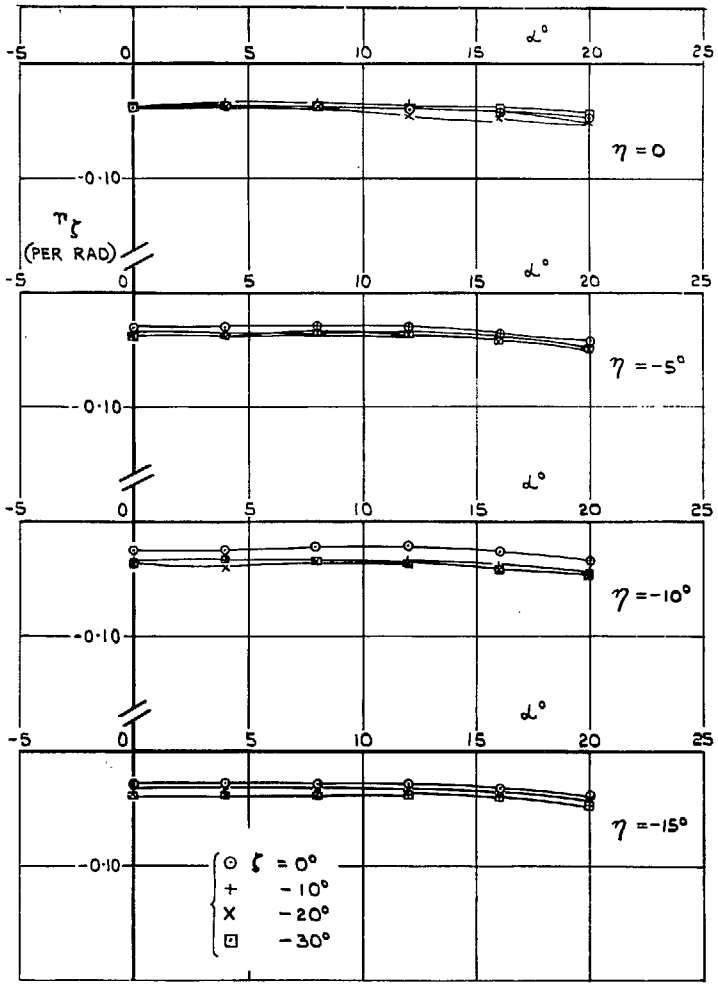

FIG. 33. Rudder-power derivative. n_ζ *vs.* α

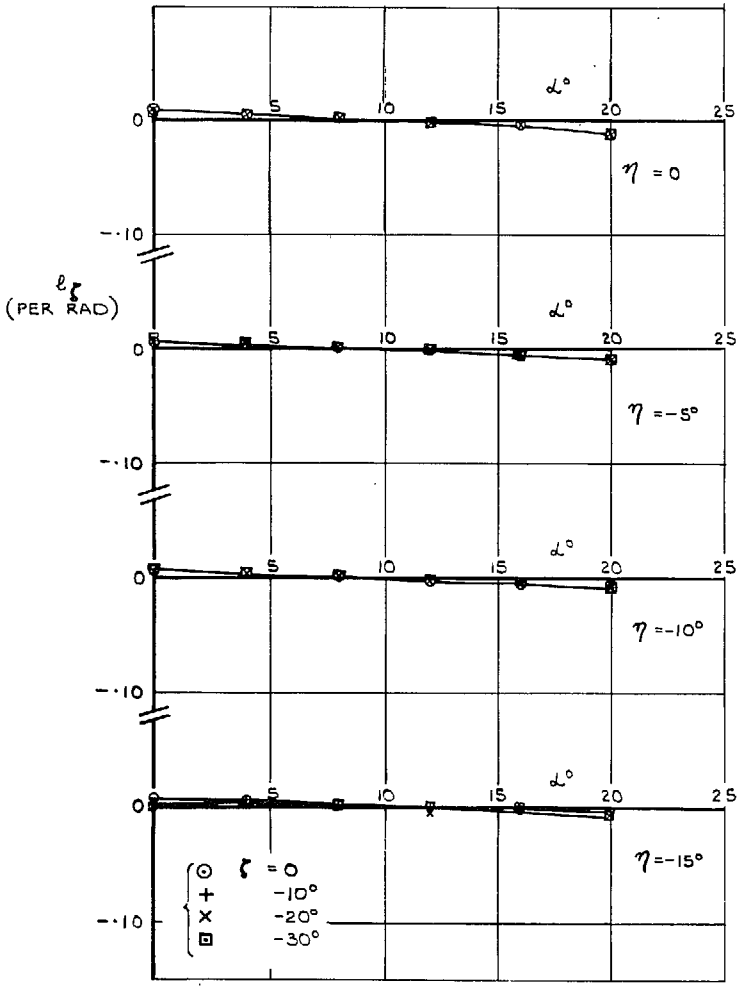

FIG. 34. Rudder-power derivative. l_ζ *vs.* α.

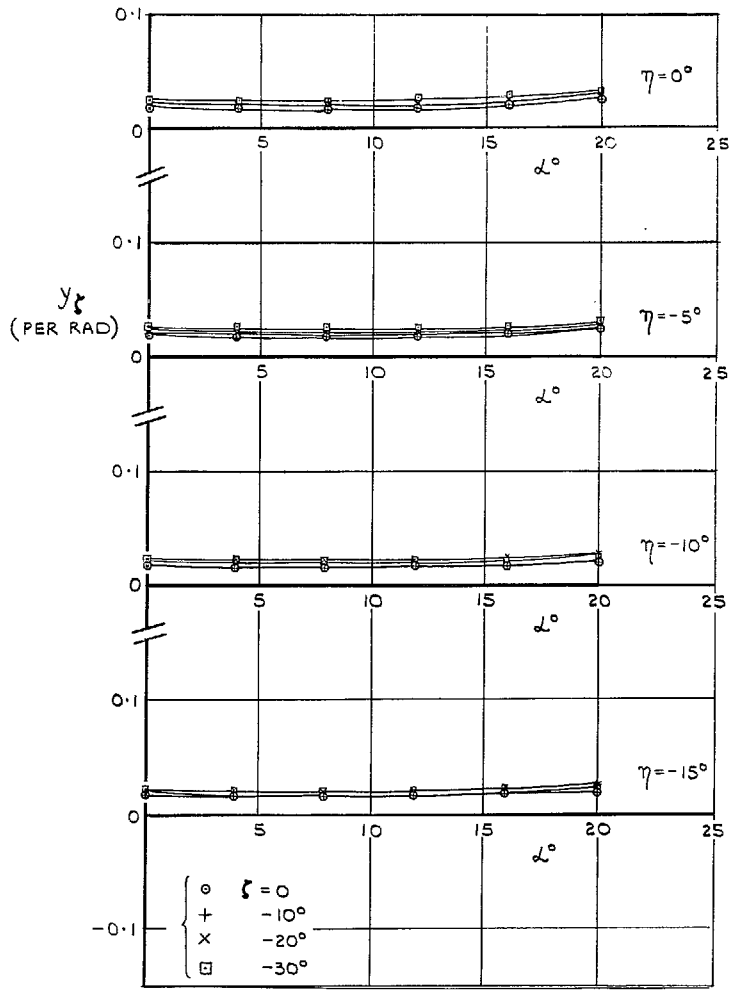

FIG. 35. Rudder-power derivative y_ζ *vs.* α.

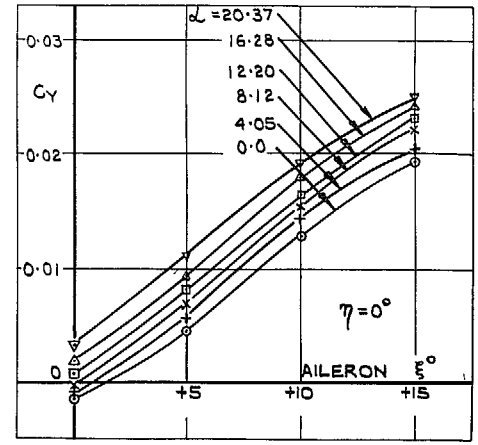

FIG. 36. $C_y \sim \xi$.

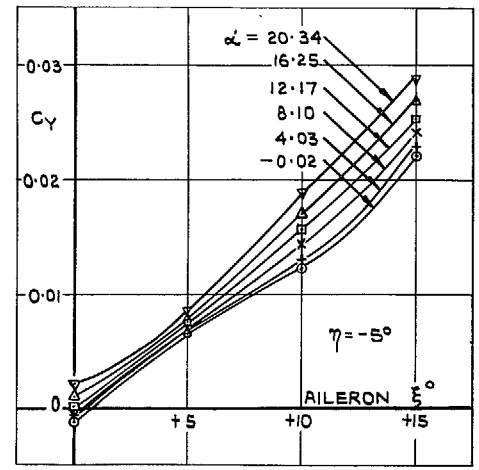

FIG. 36 (cont.). $C_y \sim \xi$.

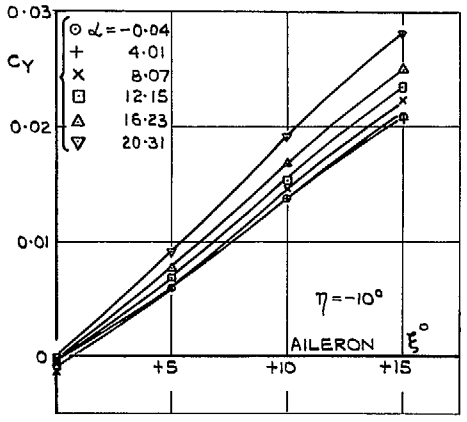

FIG. 36 (cont.). $C_y \sim \xi$.

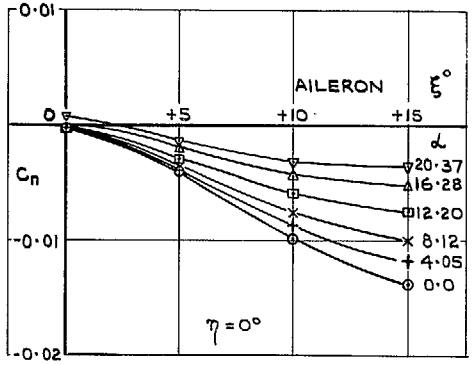

FIG. 37. $C_n \sim \xi$.

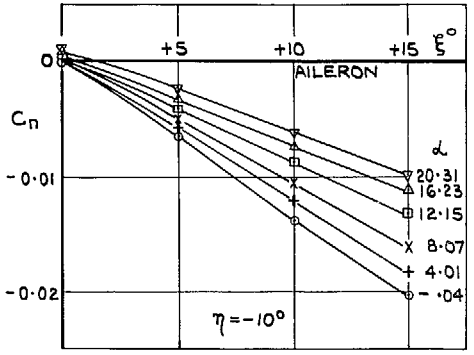

FIG. 37 (contd.). $C_n \sim \xi$.

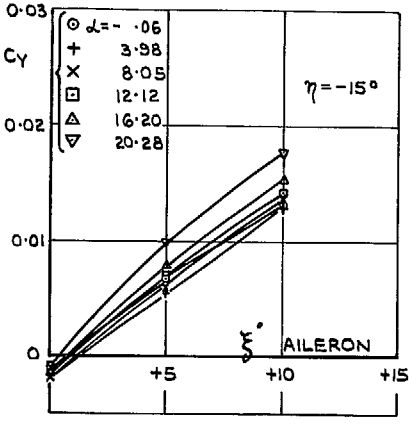

FIG. 36 (concl.). $C_y \sim \xi$.

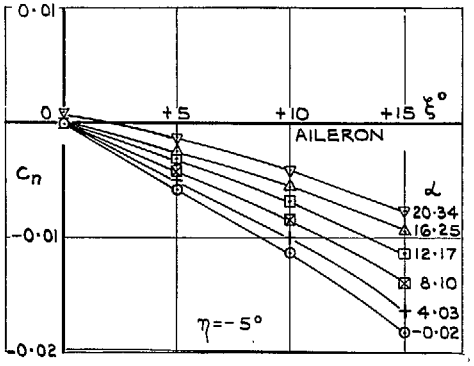

FIG. 37 (cont.). $Cn \sim \xi$.

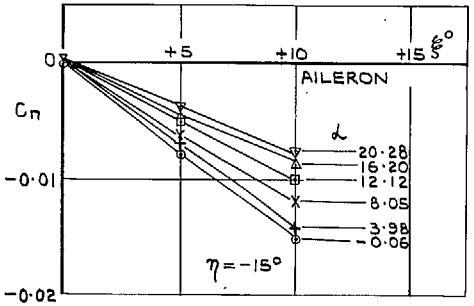

FIG. 37 (concl.). $C_n \sim \xi$.

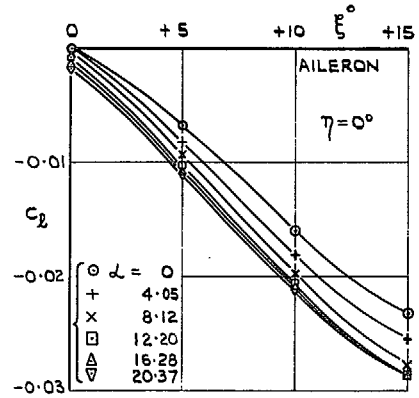

FIG. 38. $C_l \sim \xi$.

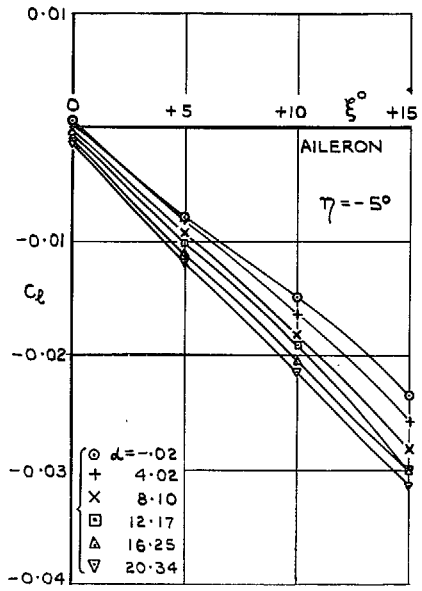

FIG. 38 (cont.). $C_l \sim \xi$.

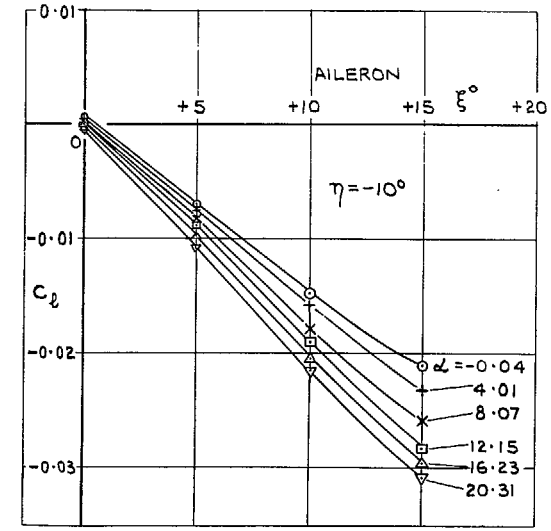

FIG. 38 (cont.). $C_l \sim \xi$.

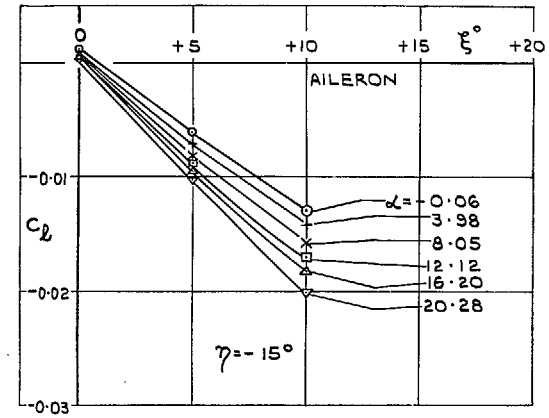

FIG. 38 (concl.). $C_l \sim \xi$.

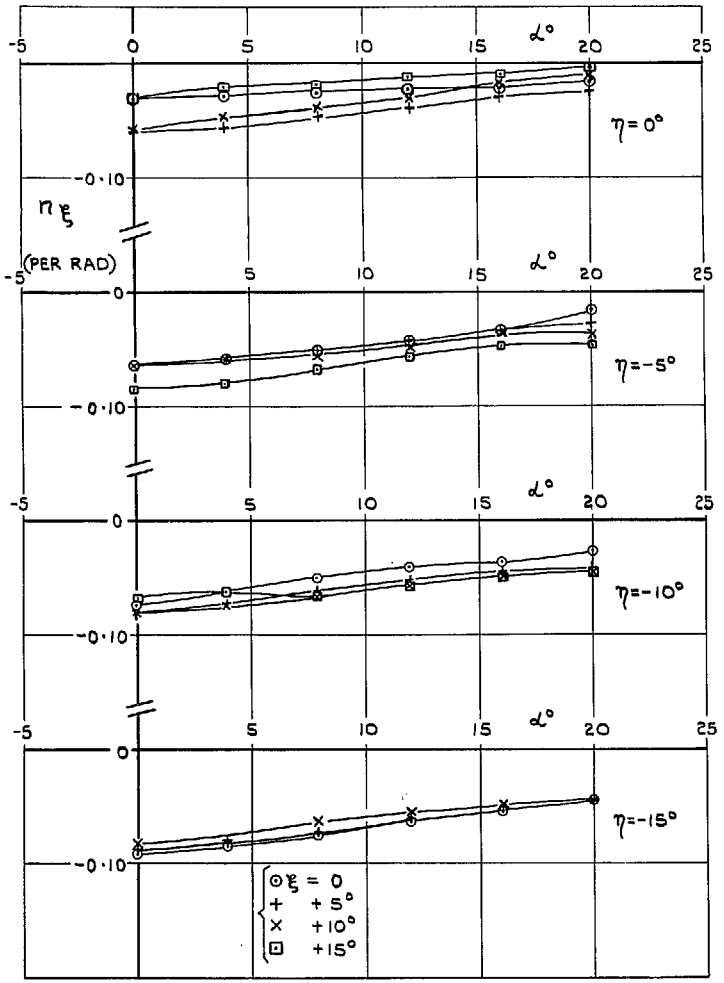

FIG. 39. Aileron-power derivative n_ξ *vs.* α.

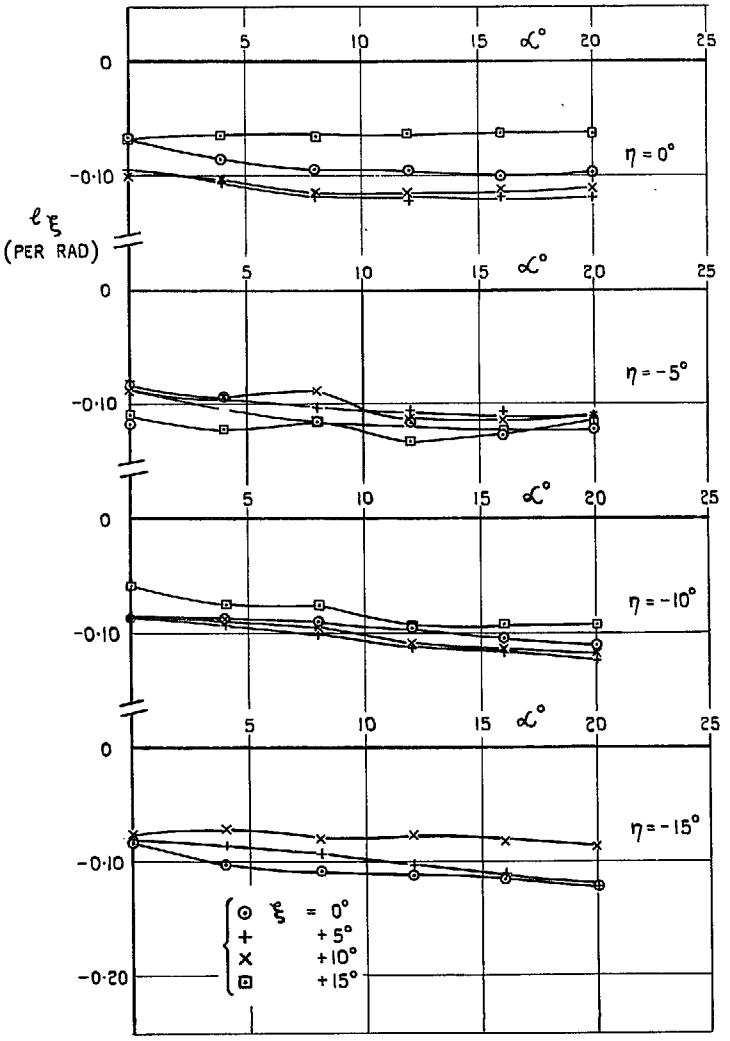

FIG. 40. Aileron-power derivative l_ξ *vs.* α.

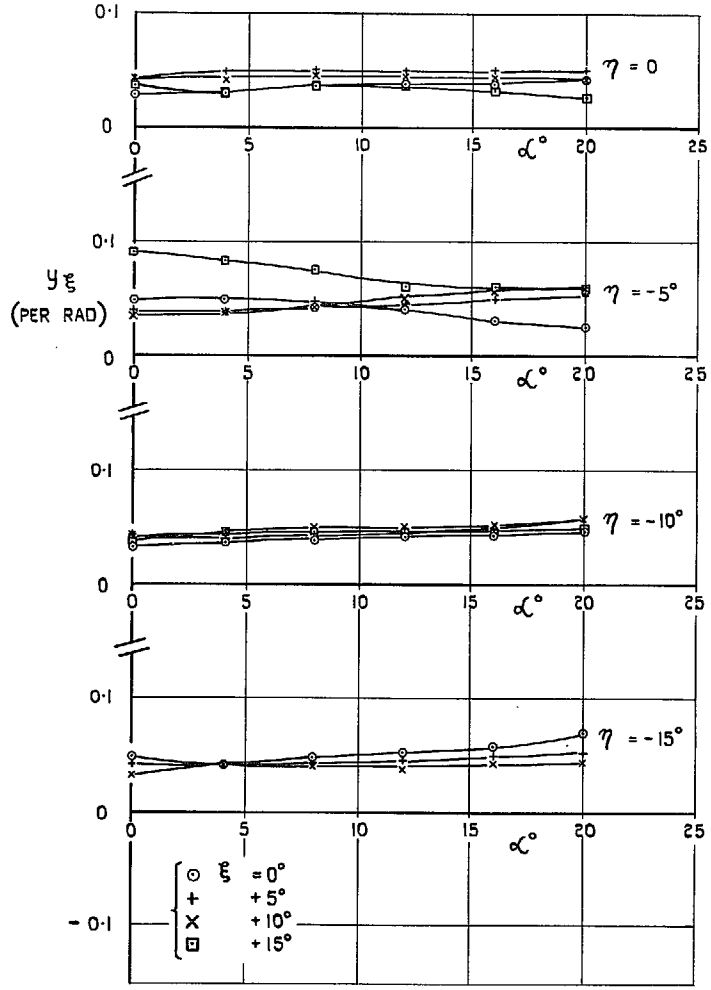

FIG. 41. Aileron-power derivative y_ξ *vs.* α.

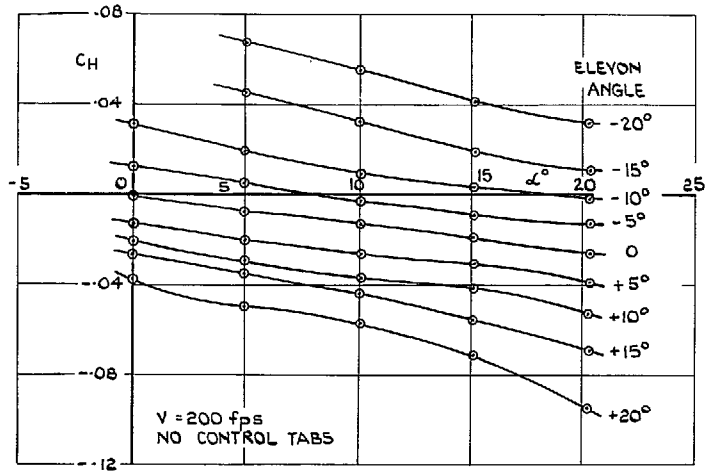

FIG. 42. Variation of hinge moment with incidence.

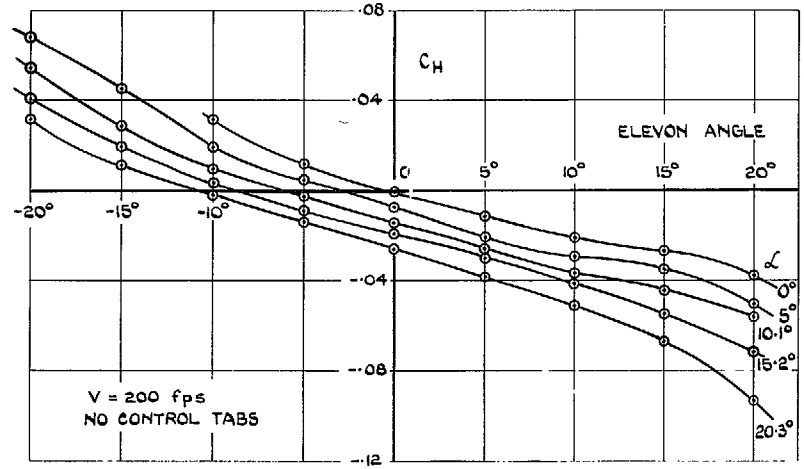

FIG. 43. Variation of hinge moment with elevon angle.

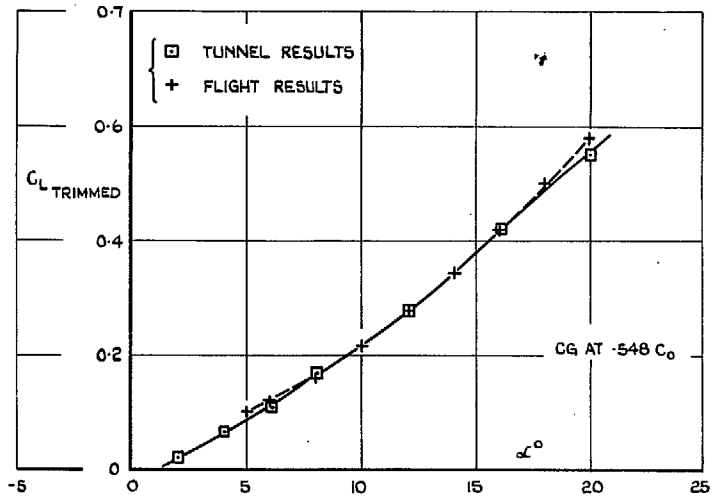

FIG. 44. Tunnel-flight comparison of trimmed lift characteristics.

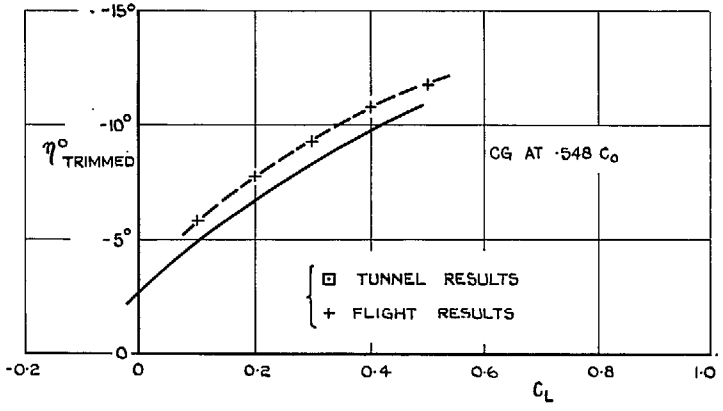

FIG. 45. Tunnel-flight comparison of elevator angles to trim.

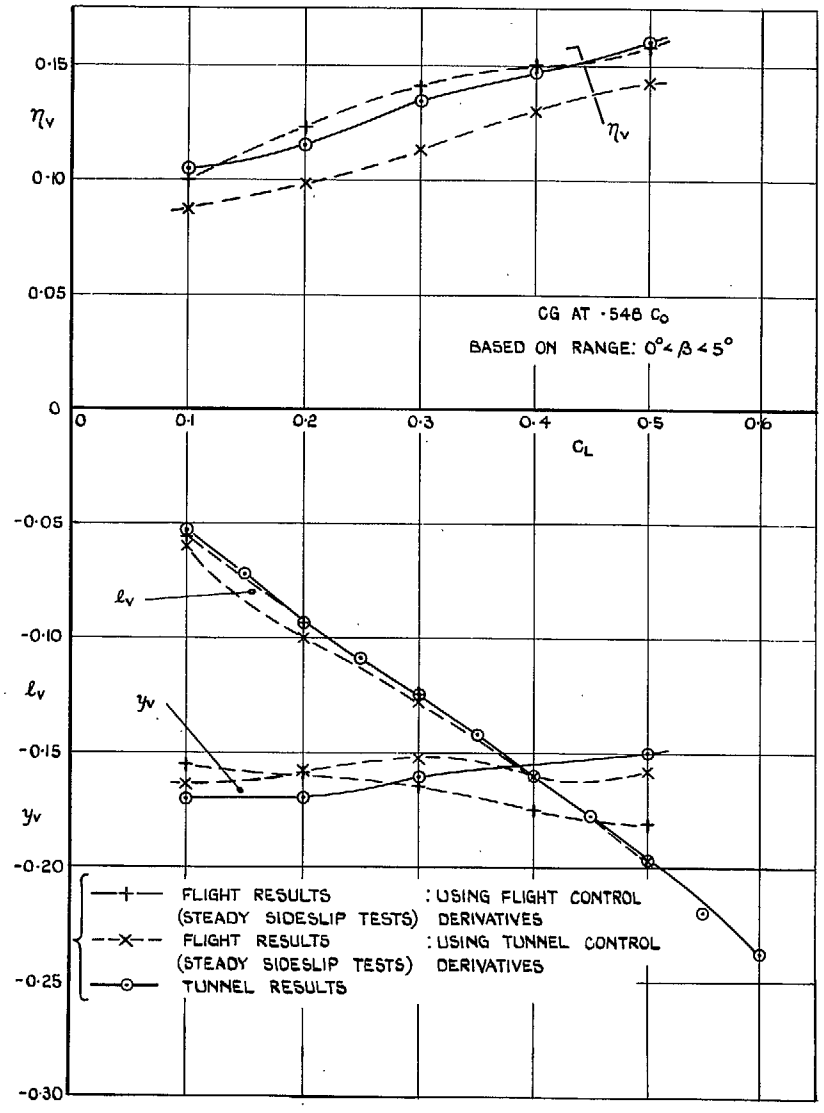

FIG. 46. Tunnel-flight comparison of sideslip derivatives n_v, l_v and y_v.

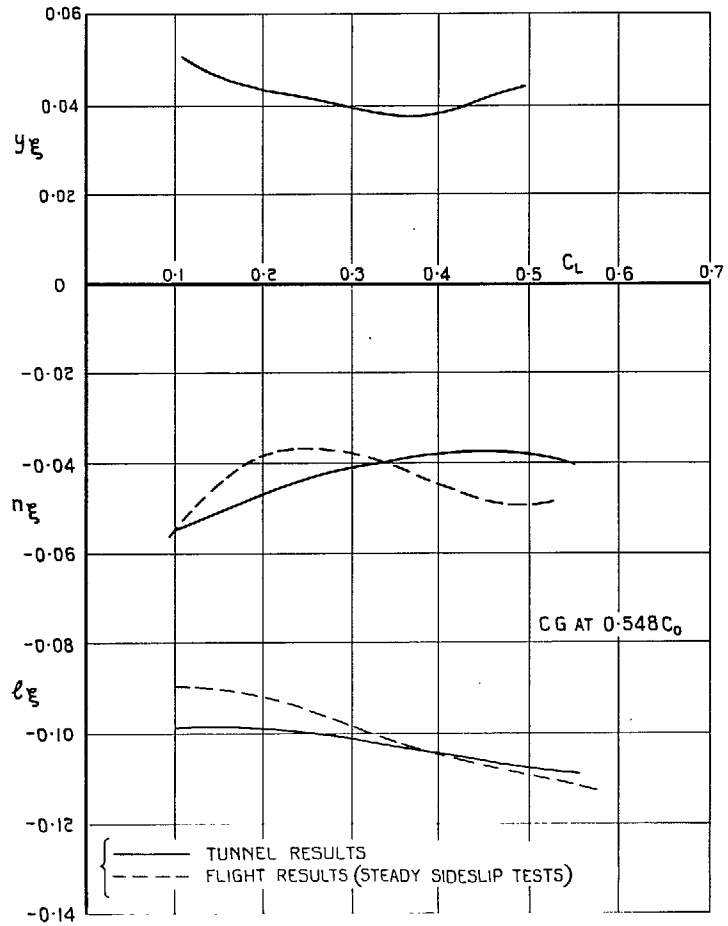

FIG. 47. Tunnel-flight comparison of aileron derivatives n_ξ, l_ξ and y_ξ.

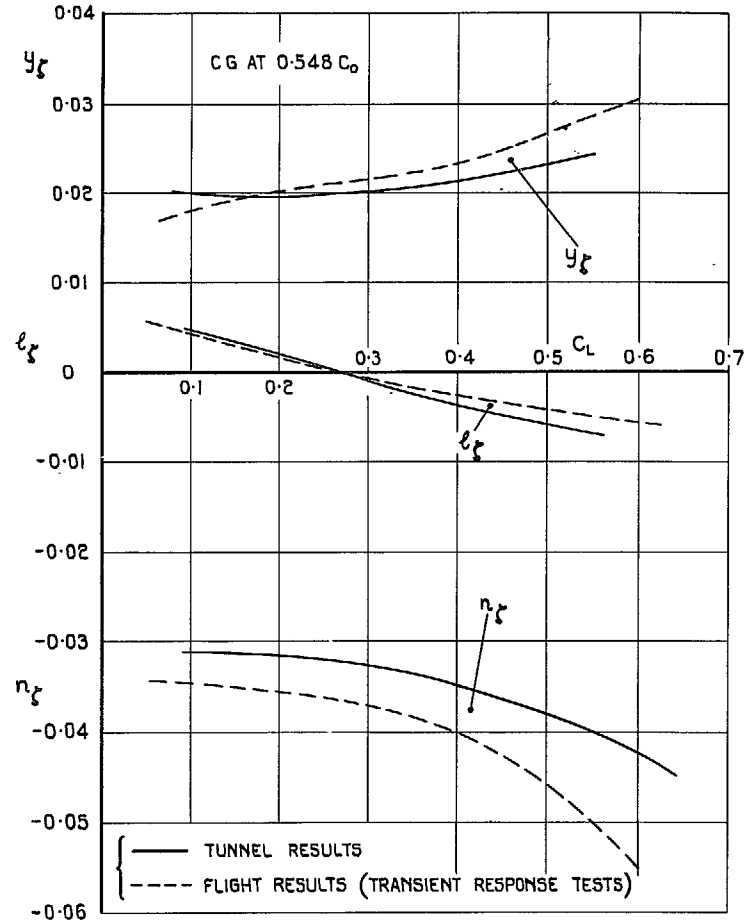

FIG. 48. Tunnel-flight comparison of rudder derivatives n_ζ, l_ζ and y_ζ.

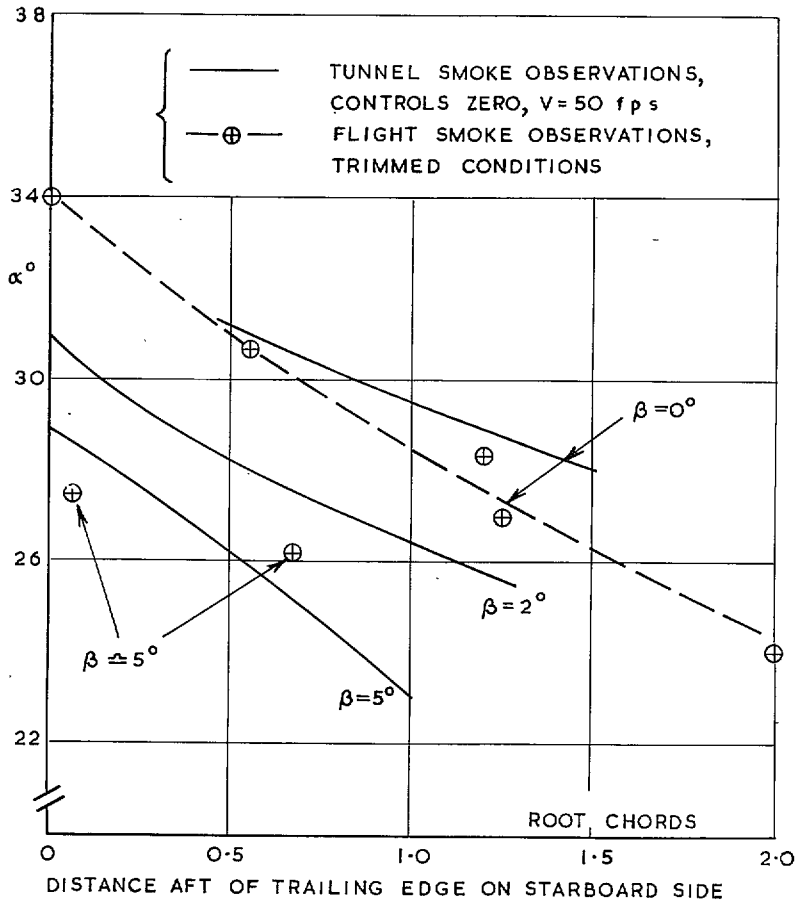

FIG. 49. Approximate position of vortex breakdown at high incidence.

Printed in Wales for Her Majesty's Stationery Office by Allens Printers (Wales) Limited

Dd.129527 K.5 7/67

Published by
HER MAJESTY'S STATIONERY OFFICE

To be purchased from
49 High Holborn, London W.C.1
423 Oxford Street, London W.1
13A Castle Street, Edinburgh 2
109 St. Mary Street, Cardiff
Brazennose Street, Manchester 2
50 Fairfax Street, Bristol 1
35 Smallbrook, Ringway, Birmingham 5
7–11 Linenhall Street, Belfast 2
or through any bookseller

S.O. Code No. 23–3486